TOPOLOGICAL DEFECTS IN NEMATIC AND SMECTIC LIQUID CRYSTALS

Bryan Gin-ge Chen

A DISSERTATION

in

Physics and Astronomy

Presented to the Faculties of the University of Pennsylvania

in

Partial Fulfillment of the Requirements for the

Degree of Doctor of Philosophy

2012

Randall D. Kamien, Professor of Physics and Astronomy
Supervisor of Dissertation

A.T. Charlie Johnson, Jr., Professor of Physics and Astronomy
Graduate Group Chairperson

Dissertation Committee
Douglas J. Durian, Professor of Physics and Astronomy
Andrea J. Liu, Professor of Physics and Astronomy
Tom C. Lubensky, Professor of Physics and Astronomy
Mark Trodden, Professor of Physics and Astronomy

TOPOLOGICAL DEFECTS IN NEMATIC AND SMECTIC LIQUID CRYSTALS

Acknowledgements

This work would not have been possible without the direct and indirect assistance of a large number of people. First, my advisor Randy has taken me under his wing and taught me much of what I know about being a scientist. The time we spend discussing many things, physical, mathematical, or miscellaneous is more valuable to me than words can express. His influence and style have greatly shaped my way of doing science and without his persistent encouragement I would not have been able to push these ideas as far as I have.

I thank also Gareth Alexander and Sabetta Matsumoto for working with Randy and me on topics related to this thesis work. Gareth in particular spent countless hours discussing this material with Randy and me and much of this thesis should be regarded as coming out of our collaboration.

Herman Gluck taught me about the Pontryagin-Thom construction which plays a large role in this thesis. He also introduced me to Fred Cohen, who spent much of his visit to UPenn teaching us homotopy theory and algebraic topology. I'm also

very grateful to Fred for his interest in our "liquid crystalline" perspective as well.

The entire UPenn soft matter group, both theory and experimental sides, has also shaped my thinking in very profound ways. I am grateful to have come to an institution with such a vibrant and active community and will surely miss it when I leave. In particular, I thank professors Andrea Liu and Tom Lubensky for their interest in my ideas and their feedback on several projects.

My officemates Ed Banigan and Jim Halverson are to be thanked for sparing me a little room on the couch and for many enjoyable discussions.

I learned much about physics and topology from Jeffrey Teo and Liang Fu. Jeffrey spent many, many hours teaching me the basics of topological band theory and also patiently listened to me struggle through half-baked early visions of this work and other projects. While I'm at it I should mention Pat Vora and Austin Joyce, who participated with Jeffrey and me in various study groups over the past few years.

I'd also like to acknowledge the other UPenn Physics graduate students, particularly those that entered with me in the fall of 2007, for many things but the details are better left unwritten here.

ABSTRACT

TOPOLOGICAL DEFECTS IN NEMATIC AND SMECTIC LIQUID CRYSTALS

Bryan Gin-ge Chen

Randall D. Kamien

Liquid crystals are materials with interesting symmetries and order, and their science and applications are a playground of geometry and elasticity. I discuss various aspects of the study of topology and topological defects in liquid crystalline systems beyond the traditional calculation of homotopy groups. I consider two problems. First, how can we better visualize three dimensional nematic orientation fields given that many experiments and simulations now are creating and manipulating configurations with complicated topology? I show that the Pontryagin-Thom construction leads to a natural set of colored surfaces, generalizing the prototypical dark brushes seen in Schlieren textures between crossed polarizers. If we are interested in properties preserved under smooth deformations, these colored surfaces can stand in for the rest of the configuration, leading to a reduction in dimensionality of the data to be considered, as well as an aesthetically pleasing representation of what's happening. The second problem is the relationship between translational order and orientational order in smectic liquid crystal systems. Smectics are liquid crystals which organize themselves into layers where the naïve generalization of the

calculation of homotopy groups leads to results on defects which are incorrect. I show that these difficulties arise from the lack of independence between translational order and orientational order. These considerations are neatly captured by a surface model of two-dimensional smectics. By looking at a smectic configuration as a graph over the sample space, the nature of the rules governing the defects and their relationship to the symmetries of the system are clarified.

Contents

List of Figures

Chapter 1

Introduction

Advances in human understanding and control of materials have driven much of the course of history – witness the names of the Stone age, Iron age, and Bronze age. However, only within the last century or so have the laws governing materials begun to be distilled into the general principles of condensed matter physics. This body of knowledge guides scientists' classification and organization of materials and their properties and inspires them to design and investigate ever more exotic and useful materials. One important theme in the study of condensed matter is that the behavior of materials is often dictated not by the properties of most of the bulk, but rather by that of its defects. This is akin to the strength of a chain being determined by its weakest link. Furthermore, understanding how materials change from one phase to another can require a knowledge of the defects which are created during such phase transitions. For instance, crystals melt around grain boundaries

and dislocations when their temperature is raised. For these reasons, the study of defects is of utmost importance in the physics of materials.

A class of materials in which defects may readily be visualized and studied are liquid crystals. As their name suggests, these are materials that have properties of both liquids and crystals. Once merely laboratory curiosities, liquid crystals are now ubiquitous in consumer devices like cell phones and laptop displays. Two phases of liquid crystals will be discussed in this work. The phase in most displays is the nematic, which is a liquid of molecular rods. The rods tend to align, giving nematics a local orientational degree of freedom. The smectic phase on the other hand is a phase made of fluid layers of molecules. The layers prefer to be equally spaced and thus form an ordered crystal along one axis which is perpendicular to the liquid-like directions within the layers.Liquid crystals present many challenges for theorists – a cavalier way of describing the duality at play is that their crystalline properties make them "hard" in that they have many interesting symmetries and thus anisotropic elastic behavior, but their liquid properties make them very "soft" in that these symmetries are easily disrupted by defect structures and their elasticity is dominated by fluctuations away from an ideal state.

As with all broken symmetry materials, liquid crystals admit topological defects, which are regions of the sample forced to be discontinuous by the topological behavior of the configuration outside of them. Such defects are stable in the sense that they cannot be removed by a purely local perturbation of the material, they

must either be moved out to the boundary of the sample or merged into other such topological defects.

Historically, topological defects in ordered media were first studied using the language of homotopy theory beginning in the 1970's, with the papers Toulouse and Kléman [1976], Volovik and Mineyev [1976] and Rogula [1976]. Following this, there was a period of great interest by condensed matter physicists culminating in several reviews, including one very influential one by N.D. Mermin [Mermin, 1979].

Most previous work on topological defects has focused on characterizing single defects by calculating the homotopy groups of the order parameter space. This idea begins with the philosophy that defects may be identified with the behavior of small measuring loops or spheres around them. Thus, the "charge" of the defect is the topological class of the configuration in the sample on such a measuring circuit. Next, one observes that there is a natural way of combining two loops or spheres by "shrink-wrapping" a larger one around them, and this leads to the algebraic structure of a group in which the different charges can be multiplied. For a discussion of homotopy groups applied to liquid crystals see Alexander et al. [2012].

This dissertation has two parts which address the theme of topological defects beyond homotopy groups. First, given the development of new three-dimensional imaging techniques and the extensive use of simulation, one might ask for more – a way of seeing more globally in a sample how topological defects and other interesting features "fit together" without needing to restrict our attention to artificial measur-

ing circuits. In chapter 2, we will explain in detail a method for visualizing the key topological features in a sample, known as the Pontryagin-Thom construction. Very roughly speaking, there are special subsets of the order parameter space so that the topology of a configuration can be completely recovered from the locations of the points in the sample where the order parameter lies in this subset. These sets include the defects but usually include other points forming lines or sheets connecting the defects together as well. This construction is one answer to the question of what the minimal amount of information one needs from a configuration in order to be able to reconstruct it topologically. After explaining the construction we work out numerous examples, primarily 3D nematic textures in the hope that this will allow the reader to experience and begin to see how this way of thinking about things will work. This chapter is based on forthcoming work with Gareth Alexander, featuring experimental data courtesy of Paul Ackerman and Ivan Smalyukh. We conclude this chapter with suggestions for applying this technique for more complicated order parameter spaces, including the biaxial nematic.

Second, the homotopy group approach is not justified when applied to smectic liquid crystals or other crystalline systems in general. In appplications to these systems, some often unstated assumptions about how to relate abstract continuous maps in some order parameter space to maps induced by configurations in the sample turn out to be unjustified. In chapter 3, we will describe how to think about defects in smectic liquid crystals, crystals, and other ordered media with broken translational symmetries. In these systems there are two classes of defects,

dislocation-type defects which may be considered to be in the same class as those described earlier, and disclination-type defects, which are more akin to critical points in the sense of local maxima, minima or saddle points. For this reason it turns out to be convenient to consider not just the configurations as maps to the order parameter space but also an associated space which contains information about the gradient of the configuration at each point as well. We will also see that the space of order parameters in these systems turns out to be singular in a certain way consistent with the existence of disclinations. This chapter is based on Chen et al. [2009] but elaborates on certain mathematical details and explains some examples for crystals as well as for smectics. This chapter will be more of an intrigue than a full review as we shall find that we run into unanswered questions much earlier.

Finally, I conclude with a summary and outlook in the final chapter.

In the remainder of this introductory chapter, we will first introduce a very basic system which exhibits topological defects, the XY model, and introduce some of the key concepts and terms that will be used throughout. It turns out that this model is equivalent to a 2D nematic, as we will explain at the end of this section. We will then explain two generalizations of ideas presented here which will be elaborated on in the two other chapters of this dissertation.

1.1 The XY model

Ordered media are modeled by functions from our physical space, the domain, to a target space characterizing the behavior of the material at that point. When the material is in a broken symmetry state, this target space is the set of values of the non-vanishing order parameter. The function from the domain, or sample space of the material to the order parameter space will be called a "configuration", or "map". We will primarily be concerned with the topology of such configurations – more formal definitions will follow in this chapter, but generally speaking two configurations are topologically equivalent if there is a continuous one-parameter family of configurations that joins the two; that is, if they may be deformed into one another without introducing any discontinuities or defects. A reference for the general philosophy of broken symmetries is Chaikin and Lubensky [1995].

Imagine a system of spins or directions at every point in a domain of the plane, that is, we have a field $\vec{s}(x) = s(\cos\theta(x), \sin\theta(x))$. What this field represents might be a local thermal average of some microscopic spins at atomic lattice sites or a similar average of local orientations of some anisotropic molecules. At temperatures low enough that the system is in the ordered phase, however, we can treat the magnitude s of the order as a constant and instead focus on the field $\theta(x)$ at each point x where θ is a point on a circle, realized, say as a point in the line such that θ is equivalent to $\theta + 2\pi$. We will use the notation $\theta : D \to S^1$ where D here is our domain, the sample space, and S^1 is the 1-dimensional sphere, the circle, which is

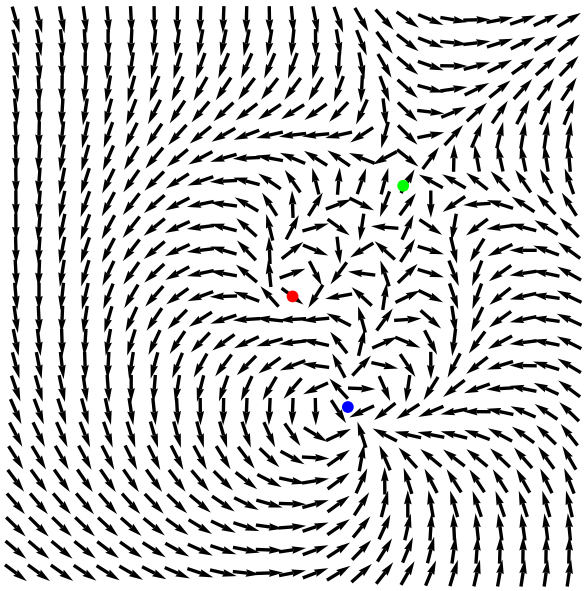

Figure 1.1: A configurtion of spins in the XY model. The vortices are labeled with colored dots.

the order parameter space for this system.

Suppose that these spins interact in such a way that nearby spins will tend to align. A simple form for the free energy of the system is therefore

$$F_{XY} = \frac{1}{2} d^2x \rho_s [\nabla\theta(x)]^2 \tag{1.1.1}$$

Note that it is possible that θ might not be represented by a single-valued field everywhere. In particular, suppose we have an annulus where $\theta = \phi$ (ϕ being a polar coordinate around the annulus). For instance, take a small annulus around the red point in Fig. 1.1. Along the line segment $\phi = 0$, there is a discontinuity in our representation of ϕ. However, this can be removed by working with local coordinates in the circle – e.g. we might cut the annulus into two pieces and let

$\theta = \phi$ in one piece and the equivalent $\theta = \phi + 2\pi$ in the other. This apparent discontinuity is sometimes exploited when integrating by parts. We bring up this point now as the issue of working in local coordinates is crucial and the idea is key to some later constructions.

The gradient of θ is large if spins are rapidly changing - we thus can restrict attention to configurations where θ is continuous except perhaps at particular points. In particular, all low-energy distortions correspond to deformations of the field θ which are continuous. Motivated by this fact, we introduce the notion of homotopy.

Two continuous maps f, g are said to be homotopic if there exists a family h_t of maps continuous in t where $t \in [0, 1]$ and $h_0 = f$, $h_1 = g$. The family h_t is called a homotopy. Homotopic maps fall into equivalence classes called homotopy classes; these are the path components of the (usually infinite dimensional) space of all functions from the domain to the order parameter space. Homotopy will be our first notion of topological equivalence and we will spend some amount of time classifying the possible configurations up to homotopy. We will often do this by first classifying the possible maps from certain measuring circuits up to homotopy.

Note that there is a one-parameter family of ground states which minimize F_{XY}, namely $\theta(x, y) = \theta_0$ with any θ_0 in the circle. The system breaks the continuous rotational symmetry; one must rotate each spin by an integer multiple of 2π before one gets back the same state. This should be contrasted with the isotropic state which has all symmetries. Working infintiesimally around each ground state we see

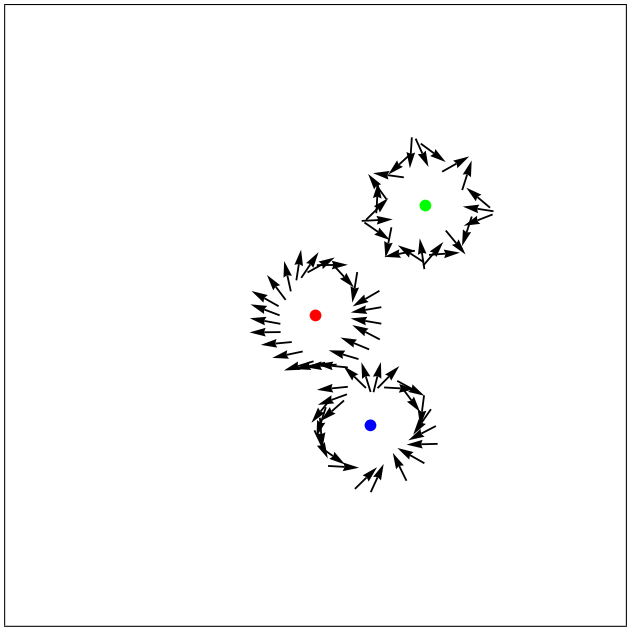

Figure 1.2: Measuring loops around the vortices in Fig. 1.1. The degree of the vortices can be determined from counting the winding on these loops. Green has degree -3, blue has degree 2 and red has degree 1.

that there should be one infinitesimal deformation which costs no energy. If this deformation is "spread out" to have a finite wavelength, this will have a sound-wave like dispersion and is the simplest example of a Goldstone mode. The ground states in this system are all homotopic to each other, but there are many configurations which are homotopic to the ground state without being the ground state, and indeed, many which cost high energy. Thus it is not true that two topologically equivalent configurations are energetically equivalent – in what follows one should always remember the caveat that the energetics must be considered as well after one has determined the classification topologically.

1.2 Defects

Suppose that our domain takes the form of a disk centered at the origin of the plane, and we require that the value of θ at the boundary is equal to the polar coordinate ϕ. In this case, we will see that the boundary conditions are inconsistent with having a continuous field θ everywhere inside the domain. At best, we can have a field continuous everywhere except at a single point. First, note that on a measuring loop or circuit running counter-clockwise and concentric with the boundary θ winds once from 0 to 2π around the order parameter circle.

Since on any closed circuit θ must return to itself up to an integer multiple of 2π, the net winding of θ on the circuit is an integer. This defines a very basic topological invariant of maps from the circle (points on the measuring circuit) to a circle (the order parameter space) called the degree. This is an invariant in the sense that two maps from the circle to the circle are homotopic if and only if their degrees coincide. This is physically obvious for anyone who has played around with or can imagine a loop of string tied around a cylinder, but for a proof see Hatcher [2002].

The above invariant is simply for maps from a circle to the order parameter circle, so it is worth spending a bit of time spelling out what knowing this on some measuring circuit tells us about the configuration in the sample. First, only when the degree on some measuring loop is zero can its interior be filled in with a

continuous configuration. This is because if $\theta(x)$ is continuous everywhere in the sample, any continuous deformation of the loop as a path in the sample induces continuous deformations of the map from the loop to the order parameter space. One valid deformation of the loop in such a sample is simply to shrink it to a single point, inducing the constant map from the loop to the circle, which obviously has zero degree. Consider for instance any loop not surrounding a colored point in Fig. 1.1.

In the above case, the degree on a circuit at the boundary is equal to one. Therefore, we cannot shrink a measuring loop continuously from the boundary to any point in the disk where θ is well-defined, as otherwise the degree would change from 1 to zero. There must be a defect point, traditionally called a vortex for the XY model, where the θ field is discontinuous. Just as regular points in the sample are characterized by having zero degree on loops surrounding them, loops around this vortex must have a degree of one. Fig. 1.2 shows the measuring loops around the vortices of Fig. 1.1.

The existence of vortices means that we must consider configurations which are everywhere continuous in the domain except at certain lower dimensional sets. A configuration with defects from a domain D to the order parameter space will be a continuous function from $D \setminus \Sigma$ to the order parameter space X. The notation $D \setminus \Sigma$ simply means D with some defect subset Σ removed from it (in the above example, D is a disk and Σ is some point inside).

The degree fully characterizes vortices in the XY model. By "spreading out a homotopy in space", we can see that two defects with the same degree are topologically equivalent in that we can replace a small neighborhood of one with a slightly smaller neighborhood of the other with a continuous annulus between them. For instance, let C_0, C_1 be circular loops around two vortices of the same degree, with the radius of C_1 slightly smaller thatn C_0. Then we can delete the disk bounded by C_0, and place the disk bounded by C_1 inside. In between, we have a missing annulus, which we can fill in by using a homotopy between the configurations on C_0 and C_1, letting $t = 0$ be C_0 and $t = 1$ be C_1.

We now know enough so that we can discuss the homotopy classification of configurations with defects in the XY model. The defect sets Σ will be sets of points (lines can be ruled out because the order parameter space is connected). Suppose then that Σ consists of n points. Notice that we can shrink a domain with n punctures to a subspace consisting of n circles joined at a point, the bouquet of n circles. This space is what's called a deformation retract of our original sample and is homotopy equivalent, meaning that the classification of maps here is identical to the one for the original sample Hatcher [2002]. With this picture, it's clear that each of these n circles can admit a map with any integer degree and that different choices of degree at each circle correspond to different homotopy classes of maps. Thus configurations with n defects are classified up to homotopy by an ordered set of n integers, corresponding to the degree around each of the defects.

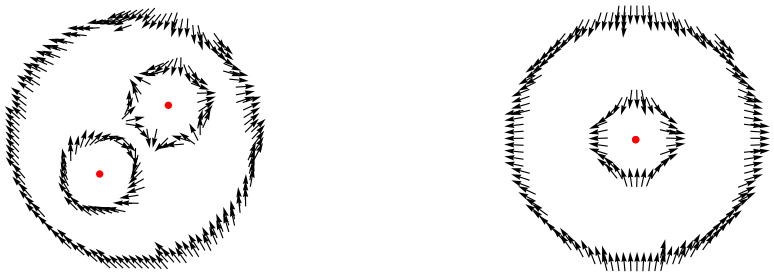

Figure 1.3: Measuring loops around a vortex of degree 1 and a vortex of degree -2 on the left, and their result, a vortex of degree -1 on the right.

1.3 Adding defects

The study of defects would not be so interesting if they were merely holes in the sample that we simply avoided. In fact, they can often be thought of as actors in their own right, merging into new defects, or splitting and giving birth to children. The laws for this more dynamical behavior is what we are really after.

The case of the XY model is instructive. Note that the degree is additive in the following way. Suppose I have two loops in some sample drawn around two defect points each of degree 1 (Fig. 1.3). If there are no other defects in this sample, we can see that a larger loop around these two defect points must have degree 2. To see this explicitly, consider the contour with the segments ab and ba running between the two original loops. The degree on this loop is clearly 2, as we have the contributions from the two original loops and the contributions from ab and ba cancel. This loop may be continuously deformed to any outer loop, so the degree of those is also 2. In general, a loop around two defects which have degree k and

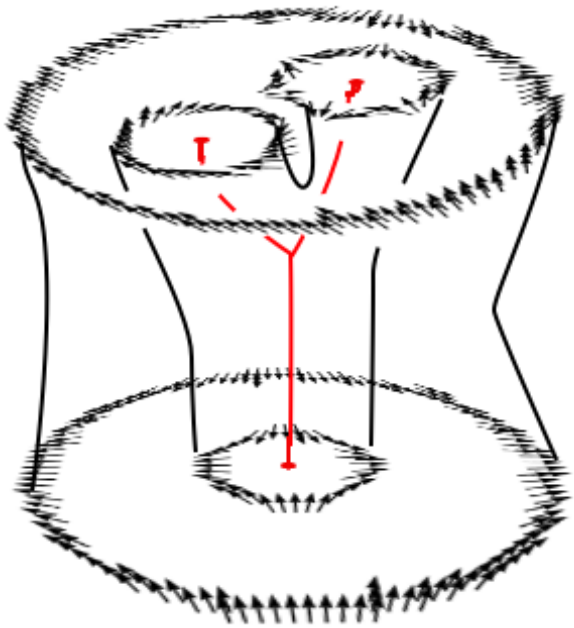

Figure 1.4: A schematic of the bordism between the defect configurations of Fig. 1.3. For visual clarity, only spins on the surfaces connecting the measuring loops are drawn. In the notation of the main text, (Σ_0, f) and (Σ_1, g) are the slices at the top and the bottom of the figure, while Σ is the red letter Y.

l has degree $k + l$, therefore it makes sense to consider adding defects as well – if we bring two vortices closer and closer together, at some point we may as well say that there is simply one defect of charge equal to the sum of its parents'. And of course such a process can be reversed; we could begin with a vortex of charge $k + l$ and split it into two vortices of charge k and l, respectively.

We can formalize this process of merging or generating vortices in a configuration with the mathematical notion of bordism (sometimes called cobordism in older literature, also called concordance in some special cases). This is a notion similar to homotopy but allows more freedom in the deformation between the beginning and ending configurations. The word arises from the root "bord-" as in "border",

and the intuitive idea is that two objects form the boundary of a space of one higher dimension. I define here bordism of configurations with defects, bordism of other objects will be introduced in the later chapters. Two configurations $(\Sigma_0, f), (\Sigma_1, g)$ from D with defects are bordant if there exists a subset Σ of $D \times [0,1]$ and a (continuous) map $b : (D \times [0,1]) \setminus \Sigma \to X$ such that the restriction of Σ to the 0-slice coincides with Σ_0 and the restriction of b to the 0-slice coincides with f and similarly the restriction of Σ to the 1-slice coincides with Σ_1 and the restriction of b to the 1-slice coincides with g. What this definition allows is for the defect set to change – for instance, a configuration with two degree 1 defects is bordant to a configuration with one degree 2 defect; the set Σ looks like a letter Y (Fig. 1.4). Another way of looking at this is that this is nothing more but a configuration defined in space-time with some defect Σ somehow interpolating between the original and final defect sets.

If all defect sets $\Sigma_0, \Sigma_1, \Sigma$ are empty, this is simply a homotopy. We therefore extend our definition of homotopy from configurations which are continuous everywhere to configurations with the same defect sets by saying that they are homotopic if they are bordant and further $\Sigma = \Sigma_0 \times [0,1]$, that is, there is no change of Σ_0 in time as it becomes Σ_1.

Let us now point out that we should supplement 1.1.1 by what happens at points of discontinuity, as at such points the gradient is not well-defined. A discontinuity is accompanied by a loss of order, and therefore physically, the spins in the vicinity of the discontinuity are melted from the ordered phase to the disordered isotropic

phase. Therefore, we may model the discontinuity by punching out a small disk, say of radius a around the disk and replacing it with a region in the isotropic phase. It can be shown [Chaikin and Lubensky, 1995] that the energy of the core scales quadratically with the degree around the defect. Therefore k defects with degree 1 around each is energetically preferable to a single defect of degree k. Further, it turns out that two defects of charge k, l separated by distance r interact with a logarithmic potential:

$$E_{el} = \rho_s \pi (k+l)^2 \log(R/a) + 2\pi \rho_s kl \log(a/r) \tag{1.3.1}$$

Here R is the sample size, and in a thermodynamically large system with free boundaries, the first term will diverge without charge balance. Thus we may think of these defects in the XY model as behaving like $+1$ and -1 elementary charges in a 2D Coulomb gas – this picture leads eventually to the famous Kosterlitz-Thouless theory of a defect-mediated phase transition.

Here is a summary of the main results about defects in the XY model. Given a sample with several points in it which are potentially defects, we can classify the configurations on this up to homotopy by giving the charge on each of the points. The classification up to bordism is simply by the total charge in the system – the sum of all the charges on all of the defects is an integer, and this is preserved under bordism. Going along with this is a fairly concrete picture of topological manipulations in this system: for instance, if we have topologically nontrivial boundary

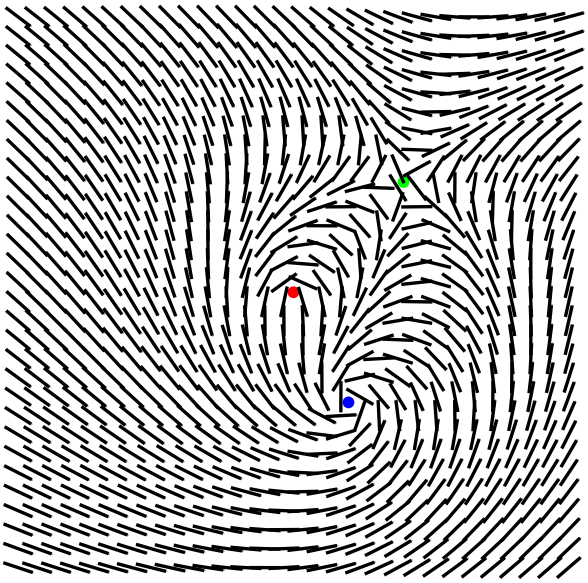

Figure 1.5: The 2D nematic configuration equivalent to that in Fig. 1.1.

conditions (meaning, inducing a nonzero degree), we must necessarily have defects in the system to cancel them out.

It turns out the XY model is actually equivalent to a model for two dimensional nematic liquid crystals. Recall that nematics are a liquid of rod-shaped molecules. A 2D nematic will refer to a system where the orientations of rod-shaped molecules are forced to lie in a plane. At each point in a 2D nematic we have a line element, just as in the XY model we have a direction. The only difference is that we need only rotate a line by an angle of π before it returns to itself, rather than 2π. Therefore we can map the 2D nematic onto the XY model simply by letting θ be *twice* the angle of the line element from the $+x$ direction (Fig. 1.5). Traditionally, the defects in the 2D nematic (called disclinations) are labelled by half the degree of the corresponding XY model vortex, as this is the fraction of a full turn that the

angle of the molecules turns around a defect.

1.4 Generalizations

The first possible set of generalizations which we will consider will be to higher-dimensional systems. That is, systems where the domain might be three dimensional, and the order parameter space might be some other higher-dimensional space as well. With a higher dimensional sample, the defect sets may accordingly be higher dimensional – they might now be points and lines in three dimensions. Accordingly, instead of measuring loops we could have measuring spheres as well.

In the main example we consider, the three dimensional nematic, the order parameter space is the space of orientations of a rod. This space is a sphere with antipodal points identified, topologically the real projective plane, in symbols, $\mathbb{RP}^2$. One cartoon of a system with nematic order is a box of chopsticks or noodles packed not too dnesely. In the nematic regime, rod shapes tend to align, but don't crystallize into well-defined layers. The ground state of all rods pointing in some direction can be disrupted by a variety of distortions and defects, the most basic being the "hedgehog" and "disclination line". Give pictures of hedgehog charge and lines here. (Chapter 2 doesn't define these)

As defects could potentially be any type of knot or link, and these are essentially impossible to classify, we shall see that thinking about bordism gives a better way

to think about such classification. Namely, we might consider charges assigned to a single loop and then give rules for how the charges change when the loop crosses or merges with other loops: a sort of generators and relations point of view.

With this order parameter space, certain special facts about combining defects in the XY model no longer hold. In the XY model, one plus one always made two; in the nematic, this is not true. One disclination line plus one disclination line can equal zero. Also important is the fact that the uniqueness of the sum of defect points in the XY model relies on the following nontrivial fact. Any bordism from configurations on two measuring circuits results in a *unique and well-defined* homotopy class of maps on the larger measuring circuit outside. In particular, we relied on the fact that all choices of the configuration on ab/ba result in the same homotopy class of the map on the resulting composite circle. We shall see that for adding point defects in the nematic that without fixing more information (e.g. choosing a basepoint), this need not be true and thus a simple-minded bordism from many defects to one is not well-defined in general. However, not all is lost, as we shall see that there are still effectively discrete charges associated to objects in the sample (in particular, now associated to possibly more than just the defects) which are combined with well-defined rules.

These issues will be developed in chapter 2, after the introduction of some new tools for visualizing and drawing what happens in these systems. The pictures in this chapter are all two dimensional and we merely had to keep track of a 2D

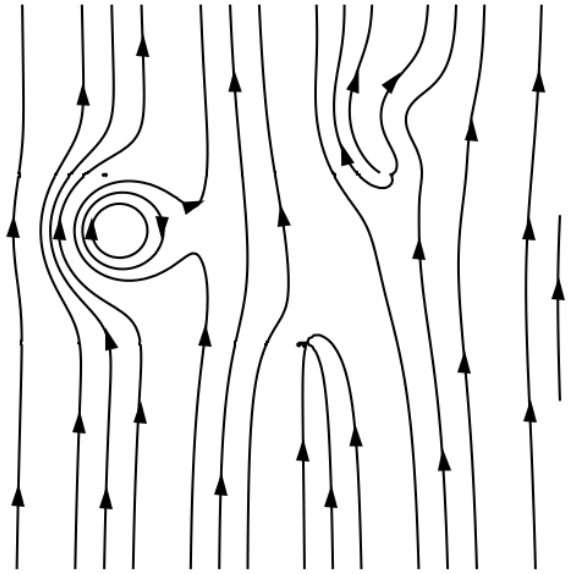

Figure 1.6: A configuration of the directed smectic. The variable θ is now a phase variable for the density waves, layers are drawn here at $\theta = 0, 2\pi$. Note the existence of two types of defects, *dislocations*, where layers are added or removed, and *disclinations*, where the orientation of the layers is ill-defined.

arrow at each point. To step up to visualizing three dimensional spins in a three dimensional sample is a difficult problem which has often been swept under the rug, but is in fact quite tricky.

The other generalization of the XY model has a bit of a different flavor. Instead of interpreting a point on the circle as the angle of a spin, we might think instead of it as phase in a density wave. In particular, consider now the following free energy, of what we will call the directed smectic:

$$F_{sm} = \int d^2x [B((\nabla\theta)^2 - 1)^2 + K_1(\nabla^2\theta)^2]. \tag{1.4.1}$$

The ground states of this free energy are not $\theta = const$ but rather $\theta = \mathbf{k} \cdot \mathbf{x}$ for

a unit vector $\mathbf{k}$. That is, θ is not constant but the gradient vector $\nabla\theta$ is. With this free energy, θ describes the phase of a layered system which resists compression and dilation as well as bending. Just take $\theta = 0, 2\pi, \ldots$ to be locations of layers in the system. These ground states break not only rotational symmetry but also translational symmetry. Two configurations only become identical when translated a distance 2π in the direction of $\mathbf{k}$. However, the rotational symmetry seems to be derived or secondary to the translational symmetry. In particular, only the translational symmetry can be made into a Goldstone mode (which in this case looks like a longitudinal wave of compression of the layers) – this despite the fact that there is a two-dimensional set of ground states.

Directed smectics also admit point defects in θ which have nonzero degree on loops around them (now called dislocations, rather than vortices). But now note that the prototypical degree 1 defect configuration $\theta = \phi$ also results in $\nabla\theta \to 0$ far away from the origin, that is, larger and larger dilations of layers, which cost more and more energy. In order for a dislocation to survive in this system, we must also include a new type of defect which allows $\nabla\theta$ to become uniform and constant again at long distances. It turns out that this is simply a saddle point in θ; since the degree of the angle of $\nabla\theta$ is also 1 on any loop around the origin, this ought to be screened by a degree -1 defect in the angle of $\nabla\theta$ nearby. We thus must consider defects not only in θ but also the angle of $\nabla\theta$. Defects of this second type, in the orientational order, are called disclinations in these systems. See Fig. 1.6 for an image of a directed smectic configuration showing both types of defects.

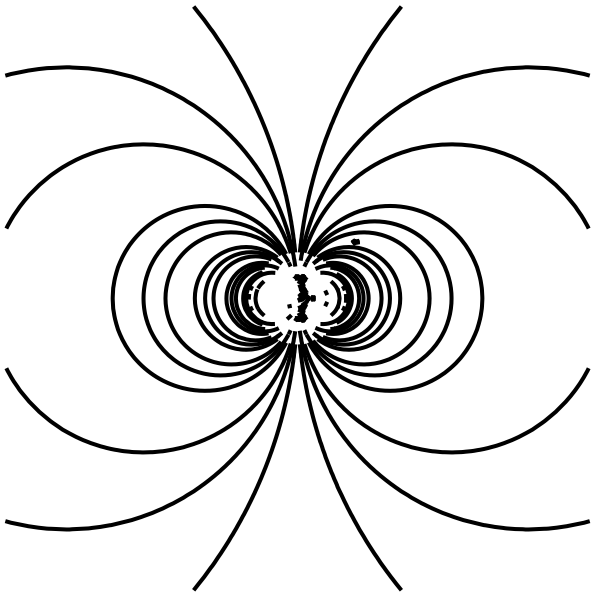

Figure 1.7: Can a directed smectic with gradient vector winding higher than +1 exist? (No.)

We will elaborate more on this generalization in chapter 3. For now we leave the reader to puzzle over the curious fact that disclinations of degree k in the angle of $\nabla\theta$ only exist when $k \leq 1$. Try to draw layers of constant θ when its gradient forms a dipole field, or any other configuration with degree higher than +1, as in Fig. 1.7, for instance.

Chapter 2

Seeing and sculpting nematic textures with Pontryagin-Thom

Nematic liquid crystals are commonplace and commerically useful in displays, optics, etc. Understanding of the geometry and topology of the molecular arrangements is key to applications and design of new devices. Furthermore, recent experiments have demonstrated a level of control which leads to several distinct complicated configurations with nontrivial topology.

Three-dimensional nematics admit both point and line defects – that is singular sets where the molecular orientation is not well defined, often forced in by boundary conditions or local frustration after quenching from an isotropic state. It can be a difficult challenge to study three-dimensional orientation fields including defects.

Current approaches to classifying the defects rely on tools from algebraic topology which may seem abstract and do not easily connect to the mental pictures that one gets from thinking about a typical sample.

The purpose of this chapter is to describe a proposal for visualizing the topology of three-dimensional nematic textures. In essence, there exists a natural set of colored surfaces in a sample which convey the topology of the line field, generalizing the brushes seen in 2D Schlieren textures.

While the Pontryagin-Thom construction is well-known to algebraic topologists, it seems that the concrete correspondence between continuous maps and bordism classes underlying it has not been widely applied to physical systems except in the case of maps to the 2-sphere.

We will use the lens of this construction to discuss the homotopy classification of 3D nematic configurations in 2D and 3D samples. As it turns out many of the complications and abstract manipulations which arise in these classification problems are pleasantly described in these terms.

In section 2.2, we recall the Schlieren textures visible when 2D nematics are viewed between crossed polarizers and connect this to the classification discussed in the previous chapter. In section 2.3 and 2.4, we present a description of the version of the Thom correspondence which is useful for 3D nematics, beginning with a discussion of 3D nematics confined in a 2D sample then explaining how defects

appear in 3D samples. In section 2.5, we present examples of surfaces generated from experimental data of a toron [Smalyukh et al., 2009]. In section 2.6, we present examples of surfaces generated from simulation for 3D nematics. The sections that follow are fairly technical and spell out some geometrical constructions which may be useful in understanding more complicated phases. Section 2.7 discusses one approach to understanding the classification of configurations with defects, due to Janich. In section 2.8, we discuss the Pontryagin-Thom theorem and describe the extension to target spaces which do not satisfy the requirements of the usual theory with an abbreviated discussion of what must be done to get a similar construction for the biaxial nematic. Finally, we conclude with a summary.

2.1 Why do we need a new visualization?

One fundamental motivation for the idea of this representation is the question "What's the minimum amount of data needed to reconstruct the topology of a texture?" For instance, in the 2D XY model, the locations of the point-like defects in the system are enough – the rest of the field configuration is uniquely determined (up to homotopy). Thus just by keeping track of the locations of points, we know what is going on and may manipulate the topological features despite there being data at every point inside the sample. One might hope that the position and charges of defects and perhaps other topological objects might similarly determine the behavior of molecular orientation fields in three dimensions, but this turns

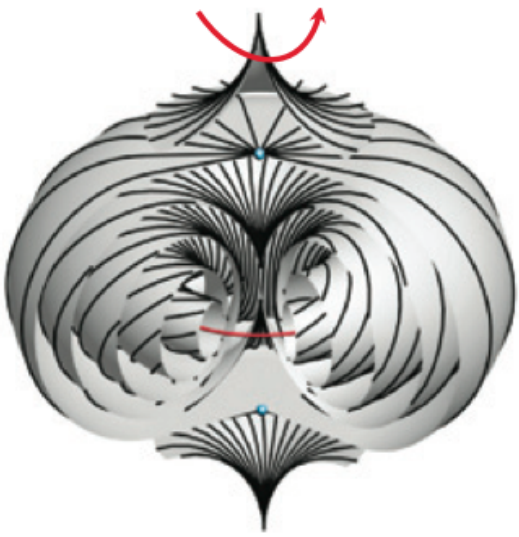

Figure 2.1: The orientation field configuration of a toron, Figure 1 of Smalyukh et al. [2009]. The blue points are hyperbolic hedgehog point defects and the red circle is the center of a double twist cylinder.

out not to work. Path-dependence of the result when combining hedgehogs in the presence of disclination lines make it hard to imagine how this could work though [Alexander et al., 2012].

Perhaps more importantly, recent experiments and simulations on liquid crystal systems have been probing textures with more and more complicated topological and geometric properties. One impressive recent example is Tkalec et al. [2011], where arrays of colloids with homeotropic boundary conditions induced defect lines in nematic liquid crystals which then were manipulated and rewired with laser tweezers into specified knots and links. Given the nearly endless topological classes that now may be programmed into the defects, one asks, what can happen in the orientation field outside the defects? It probably isn't a winning strategy to plot

line elements at each point, as one just ends up with a dense forest of sticks. A nematic configuration with an intricate structure (discussed in Section 2.5 of this chapter) is the toron, discovered in Smalyukh et al. [2009], a triply-twisted texture in cholesterics. The reconstructed orientation field from Smalyukh et al. [2009] is shown in Fig. 2.1, and is quite complicated to visualize, despite "only" having two defects.

When faced with a visualization problem with "too many dimensions", the natural impulse is to reduce the dimensionality, either by projecting or slicing the data set in some way. Instead of slicing the physical space of the sample, the domain, the key idea in this chapter is to slice the target space – here, the space of possible molecular orientations. One familiar example is that of the patterns of dark brushes observed when viewing a thin film nematic under crossed polarizers. Whenever the molecular orientation is **not** parallel to either polarizer direction, light may pass through – the remaining dark brushes thus signal that the orientation of the molecules is close to either the polarizer or analyzer direction. The points where the brushes meet or pinch off are topological defects, disclinations, and the number of brushes entering a defect is readily seen to be related to the winding number of the orientation field around that defect. Thus just by keeping track of the brushes (a one-dimensional set) we can understand what happens in a two-dimensional system.

Does there exist a generalization of this to three dimensions, where we might need only the shape of some lower dimensional set in our sample? The answer,

as we shall *see*, is yes. We will be able to use *colored surfaces* to deform three-dimensional configurations and get a feeling for the way that defects determine the topology of the orientation field around them, for instance.

I now comment briefly on the relationship of the techniques used here and the more algebraic ones explained in e.g. Mermin [1979]; Alexander et al. [2012]. In very broad terms, what we are considering are "homotopy classes of maps", that is, equivalence classes of continuous mappings from our domain space to the target space. In certain favorable cases, these sets carry an additional group structure, that is, there may exist a natural way of combining two maps to get a third, along with an identity and inverses. The techniques of algebraic topology focus on elucidating and exploiting such algebraic structures in order to shed light on the classification problem. The more constructive techniques described here allow one to draw pictures of representatives of these classes and consider other ways of combining maps which may not quite form a group (in that identities and inverses may not always exist) and yet see what the result might be.

2.2 Schlieren Textures

One prototypical liquid crystal texture is the Schlieren textures that are found when placing a thin 2D sample of nematic between crossed polarizers. In this section, we will assume that the director has planar anchoring with respect to the top and

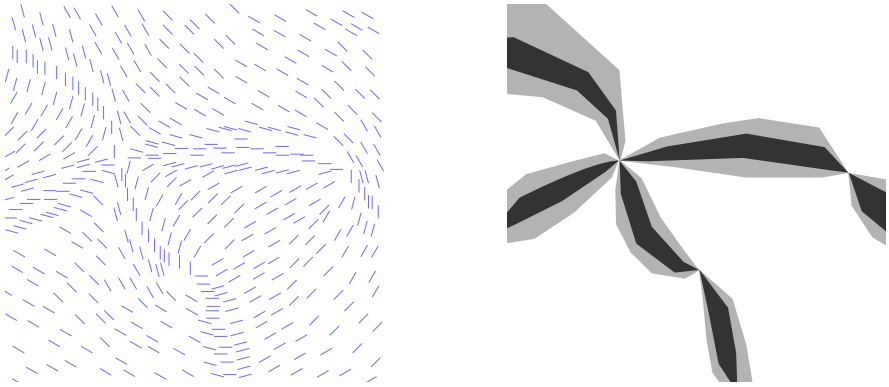

Figure 2.2: A sketch of a 2D nematic director field and its corresponding Schlieren texture.

bottom walls of the sample and that the director will therefore lie in the xy plane. One sees a characteristic set of dark "brushes" whenever the director happens to lie parallel to either the polarizer or analyzer directions, as in Fig. 2.2.

The brushes meet in certain singular points, which are interpreted as disclination defects where the orientation of the director is not well-defined. By counting the number of brushes about a point, we can determine the charge of the defect, and if we may watch the picture as we rotate the polarizer and analyzer individually, we may even determine the sign of the defects. The brushes thus give us a coarse picture of the director orientation in the sample – as I will explain below, in fact, all of the *topological* properties of the 2D director (in other words, those which are preserved up to continuous deformations, or deformations which do not introduce defects) are carried by the brushes.

Note that the brushes are generically one dimensional. If we happen to choose a point for which a two dimensional region is darkened (e.g. if the nematic director is

uniform and look at the inverse image of that direction), then we can perturb the choice of point or the configuration and recover a set of 1-dimensional curves.

Let's write out in symbolic form what the brushes really are. The director field inside the sample is the following function:

$$f : \text{sample} \to \text{set of possible directions}$$

The set of possible directors in this case corresponds to the set of lines in the plane that pass through the origin, which may be coordinatized by their angles from the x-axis, taking values in the interval $[0, \pi)$ where 0 and π are identified. This is the space $\mathbb{RP}^1$ with the topology of a circle.

Suppose that the polarizer and analyzer are the vertical $\updownarrow$ and horizontal $\leftrightarrow$ directions. Then the brushes are all the points in the sample which are mapped onto these two points in the space of directions. Symbolically:

$$\text{brushes} = f^{-1}(\updownarrow) \cup f^{-1}(\leftrightarrow)$$

I write the inverse f^{-1} because considering the brushes goes from $\updownarrow$ and $\leftrightarrow$ from the space of directors back to points in the sample, which is the inverse of the direction of the function f.

The set of brushes is thus the union of two different sets – it turns out to be con-

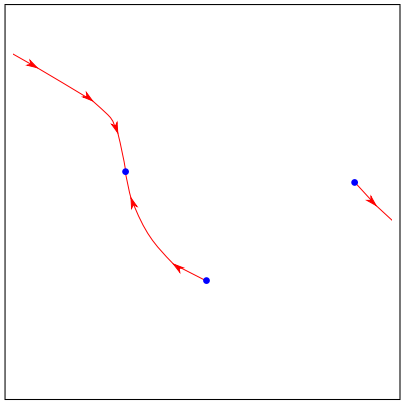

Figure 2.3: The inverse image set $f^{-1}(\updownarrow)$ corresponding to Fig. 2.2.

ceptually cleaner (and more closely related to the surface construction) to consider just one of these. Polarizing microscopy techniques are effectively able to image such "inverse image" sets as well.

Fig. 2.3 shows the picture of $f^{-1}(\updownarrow)$ corresponding to Fig. 2.2, with certain natural orientations on the curves. These orientations are defined as follows. By definition, the director at any point on the curves is $\updownarrow$. Now consider moving away from this point in the sample. If we move along the tangent direction to the curve, then the director will stays constant and equal to $\updownarrow$. However, any other direction will take us away from the curve, and the director will tilt either counter-clockwise $(+)$ or clockwise $(-)$ from the vertical. Thus the curve has a $+$ and a $-$ side, and we may choose a right-hand-rule-like convention to choose the orientation of the curves. These two sides also tell us how the brushes deform if we tilt our polarizer and analyzer away from the vertical. In Fig. 2.3, we have chosen a convention where the $+$ side of the curve lies to its right if we follow its orientation.

Figure 2.4: Switching moves: oriented curve pictures that are related by replacing a small patch of the picture resembling the patches on the left by the ones on the right (or vice versa) correspond to configurations related by homotopy.

These arrows encode the sign of the winding that the director makes around any defect. It can be checked that with the above conventions, the signed net number of arrows coming out of a defect point (divided by 2) is equal to the usual strength of that defect; for instance, by comparing figures 2.2 and 2.3, we see pictures of the 2D line field around a two +1/2 defects and a -1 defect and its corresponding oriented curve description. Further, our previous discussion of the degree of a map on a measuring loop can be viewed in this light as well. The degree is merely the (signed) number of times the oriented curve intersects the measuring loop; if a measuring loop surrounds some defects, it must intersect the net number of oriented curves leaving or entering that set of defects. Merging and splitting of defects also has a pictorial representation which makes the summing of charges clear. Two charge 1 defects merging is simply two oriented curve endpoints with arrows coming out of them joining into a single point with two curves leaving it. In terms of cancelling out opposite sign defects, endpoints of the oriented curves can merge together, forming closed loops (which we shall see can be shrunk away), or an oriented curve could also shrink in length until its two endpoints coincide, cancelling out in another way.

The equivalence between "oriented curve pictures" and 2D nematic director fields

Figure 2.5: The orientation fields corresponding to the switching moves in Fig. 2.4. For the disappearance of a bubble, the region inside the vertical circle rotates counter-clockwise through $\updownarrow$ – a similar rotation occurs for the saddle-type picture.

in a 2D sample is perhaps the simplest case of the *Pontryagin-Thom correspondence* in algebraic topology. For our purposes, it gives a one-to-one correspondence between the following two sets:

(1) All possible 2D nematic director fields in the sample, up to continuous deformations (that is, considered equivalent if there is a continuous deformation taking one to the other).

(2) All possible pictures of oriented curves in the sample, up to continuous deformations of the curves *plus* the switching moves depicted in Fig. 2.4:

The existence of the switching moves can be understood as follows. If we perturb a nematic director field in a continuous fashion we should certainly expect the corresponding oriented curves to wiggle a bit. However, during this perturbation, the curves might cross or rejoin as well, so we must keep track of such possibilities as well. For example, Fig. 2.5 depicts the line fields corresponding to the two sides of the switching moves. The reader should check that they can be deformed to one another without introducing any new defects, despite the fact that the oriented lines have apparent singularities as these deformations are performed.

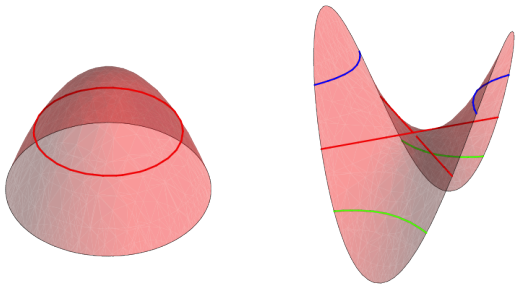

Figure 2.6: The bordisms corresponding to the switching moves in Fig. 2.4. The auxiliary time dimension is shown as the z-direction. $t = 0$ and $t = 1$ are the top and bottom slices of the surfaces; the critical slice where the topology of the oriented curves changes is colored red.

Note that these switching moves constitute bordisms of the oriented curve sets. In fact, if one draws a homotopy of the configuration in three dimensions, we can see that the oriented curves become a directed surface. More formally, two oriented curves sets $l_0, l_1 \subset D$ are bordant if there exists an oriented surface $L \subset D \times [0, 1]$ such that $L \cap D \times 0 = l_0$ and $L \cap D \times 1 = l_1$. The two switching moves correspond to a maxima / minima and a saddle point, respectively, in the bordisms between the oriented curves (Fig. 2.6). As we mentioned in the introductory chapter, homotopy is a special case of bordism of defects; here looking at the oriented curves shows that in fact, homotopy can be viewed as bordism of the subsets of the sample where the configuration is pointing in a certain direction.

The bordisms also relate the sets of curves that we get from looking at other (generic) choices of the image point rather than $\updownarrow$.

I've already explained that to get from (1) to (2), we look at the inverse image of some direction, e.g. $\updownarrow$ and assign orientations to the resulting curves from the

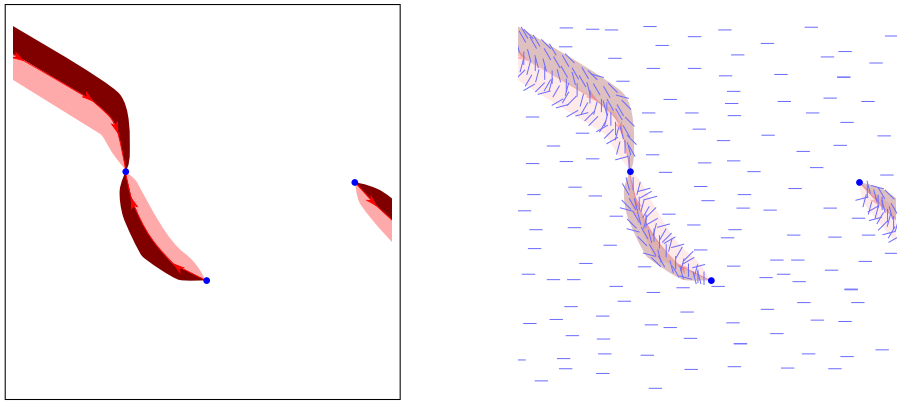

Figure 2.7: Given Fig. 2.3 it is possible to reconstruct a configuration up to homotopy.

behavior in an infintesimal neighborhood. Next suppose I wish to share an interesting texture with a colleague without having to draw a dense forest of lines. I might simply draw the oriented curve picture (Fig. 2.3) and communicate that to my colleague. But how does my colleague then recover a nematic director from this, i.e. what is the procedure for going from (2) back to (1)?

Most of the solution has already been described. The first thing my colleague does is choose a small neighborhood of the curves, as on the right of Fig. 2.7. These bubbles around the curves pinch off at the defect points, where the director is not defined. The nematic director that my colleague will construct is going to be constant outside of these bubbles, and let us choose it to be the point $\leftrightarrow$. Note that the space of directions minus the point $\leftrightarrow$ is topologically the same as an open interval, and so what my colleague does is map cross sections of the bubbles onto this interval, as on the right of Fig. 2.7.

We may thus interpret the oriented curves as a compression of the topologi-

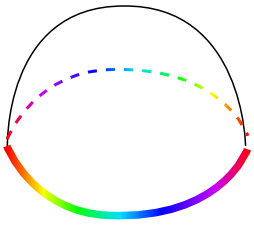

Figure 2.8: The 3D nematic order parameter space $\mathbb{RP}^2$ with the points on its equator colored.

cally "interesting" behavior of the nematic director onto a lower dimensional set. Another way of thinking about the oriented curves here is to let the angle of the nematic director be equal to (half) the phase of a complex function. Whenever the phase passes through 2π, any description of the complex function requires a branch cut. These branch cuts join zeros and poles of the complex function, and are also sufficient to reconstruct the complex function up to homotopy.

2.3 3D Nematic: 2D Sample

If the director is allowed to tilt out of the plane, the space of directions changes from the half-circle with endpoints identified ($\mathbb{RP}^1$) to the half-sphere with antipodal points on the equator identified ($\mathbb{RP}^2$) shown in Fig. 2.8. For Schlieren textures, the oriented curves were defined to be the inverse images of some particular point on the half-circle. For a 3D nematic orientation field f, we instead look at the inverse image $f^{-1}(C)$ of a non-contractible curve C, for instance, the equator, or

any other great circle. This set C is one-dimensional instead of zero-dimensional, so the inverse image $f^{-1}(C)$ also carries one parameter of data, namely the angle of the director along C. We could treat this data as a map to $\mathbb{RP}^1$ as in the previous section and thus mark the points on $f^{-1}(C)$ which get mapped to some point on the circle, but we will instead color the points of $f^{-1}(C)$ according to their angle. Supposing C is the equator, this can be done in two steps. First, find the surfaces $f^{-1}(C)$ in the sample where the director has no z-component. This can be done simply by looking for where the dot product of the director with the unit vector $\mathbf{e}_z$ vanishes. Second, color the points on $f^{-1}(C)$ according to the angle of the director in the xy-plane. If one sets the hue of the color equal to the angle from the $+x$-axis divided by 2π, one gets a pattern where all points pointing along the x-axis get colored red, and as the angle increases, the colors change as on a color wheel, until violet becomes red. Here again our caveat about generic choices holds. If f goes to a constant director and we choose to look at the preimage of a great circle which runs through that constant, $f^{-1}(C)$ will be full dimensional and not be generic. Under a small perturbation of either f or C, the generic behavior is recovered.

I will first describe some examples for configurations of 3D nematic in 2D samples, meaning that each point in a 2D sample is assigned a line pointing in three dimensions. These configurations might come from slicing a 3D sample somehow or a very thin cell with free boundary conditions on the top and bottom surfaces. First let's try to understand the dimensionality of the inverse image sets. As in the previous section when finding the $+$ and $-$ sides of the oriented curves, consider any

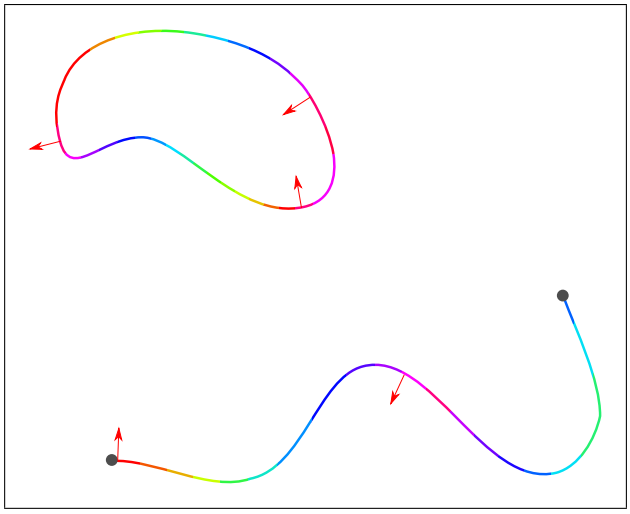

Figure 2.9: The colored lines appearing in a 2D configuration of a 3D nematic. The configuration contains two disclination defects and a skyrmion. The red normal to the curve is a local orientation of the colored lines; as $\mathbb{RP}^2$ is nonorientable, a global orientation as for 2D nematics does not exist.

point p in the sample which is mapped to the color red. Looking at a neighborhood of the colored belt in the half-sphere, we see that there is one transverse direction (as we are looking at a one-dimensional object in a two-dimensional space), thus the point p will generically have one direction in its neighborhood which will take us off of the colored belt and one direction in which the color will change. Therefore, in a 2D sample, the inverse image set must be one dimensional.

Fig. 2.9 shows a sketch of a generic "colored line" picture, which shows a colored line running between two defects and a closed loop. The two defects are visible as end points of the colored lines – this is in line with the fact that the director cannot be defined there. Furthermore, consider a measuring loop encircling a defect point. The director traces out some loop in $\mathbb{RP}^2$, and if the defect is topologically stable, this loop is non-contractible. Recall that noncontractible loops in $\mathbb{RP}^2$ are precisely

those that reverse the orientation of a point, that is, if we were to lift the loop from the half-sphere to the full sphere, they would join antipodal images, rather than close up. This implies that they generically intersect our chosen loop an odd number of times – thus the measuring circle necessarily intersects the colored lines an odd number of times.

In addition to the color on the lines, we also need an analogue of the arrows that we drew in the previous section to encode the how the the director field changes as we move off the colored lines. There we were helped by the fact that the vertical direction had two sides, a counter-clockwise side and a clockwise side, and we could globally label the two sides of the oriented curves with these as well.

In this case, $\mathbb{RP}^2$ is nonorientable, so that a global choice of $+$ and $-$ "sides" around the colored lines is impossible. In particular, a neighborhood of any great circle on $\mathbb{RP}^2$ is actually a Möbius strip.

We can also see this as follows. Imagine that we begin at the color red in Fig. 2.8, and move the director slightly away from the equator in a direction that we denote $+$. Upon following the colored line from red, orange, yellow, green, blue, violet, back to red, we find that the director is now pointing at $-$ rather than $+$. This implies for instance that any closed, colored loops in the sample must carry an *even* number of color windings, as if there were an odd number, we would necessarily find that if we thought the outside of the loop were $+$, by the time we returned it would be $-$, which signals that there is actually a discontinuity in the picture.

There is no way around it, we can only track the orientation locally, rather than globally. The least cumbersome way of doing this that I've found is to choose some arbitrary "color", say red, pick a convention for + and − in the neighborhood of red, and then label the neighborhoods of all red points in the sample. This is already shown in Fig. 2.9. Because of the lack of a global orientation, we see that the only invariant of singular points in 2D samples is the parity (even or odd) of the number of lines coming out; consistent with the fact from homotopy theory that $\pi_1(\mathbb{RP}^2)$ is the two-element group $\mathbb{Z}_2$.

What then, is the interpretation of a closed colored loop with 2 color windings? The answer is that it is the image of an escape into the third dimension, (sometimes called a skyrmion texture). Along the colored loop, the nematic director winds around the equator of $\mathbb{RP}^2$ twice, and within the center of the loop, the director points out of the plane until it is vertical. An equivalent interpretation is that (half) the color windings correspond to the number of hedgehog charges carried inside a texture.

Observe that a loop with no net color winding may be deformed to nothing, as in the case of the comparable Schlieren textures. But the loops carrying nonzero color winding are topologically stable. If we were to try to shrink them away, points with different colors and hence different orientations would run into each other, creating a discontinuity.

The switching moves for colored lines look almost exactly the same as in the

previous section – the only thing to note is that lines may only be reconnected at points where they are the same color and also have the same sign in their neighborhoods. We obviously can't cross lines with different colors because the directors are pointing in different directions in that case.

The Pontryagin-Thom correspondence here implies that there is a one-to-one correspondence between homotopy classes of 3D nematic director fields in a 2D sample and locally-oriented colored lines in that sample taken up to switching moves. To go between them, we have obvious analogues of the inverse image and bubble-filling constructions explained in the previous section. One intuitive picture of this is that we are tracking the nematic director only on a 1D space $\mathbb{RP}^1$ in its original 2D space $\mathbb{RP}^2$, and this compresses the data in the 2D sample onto (arbitrarily small neighborhoods of) a set of 1D curves.

We can now use this to classify 3D nematic configurations on a 2D sample with no defects. Suppose that we have constant boundary conditions so that no colored lines run off to infinity. The only topologically stable colored lines are those loops carrying color winding (necessarily even). The switching moves allow us to join them all into one big loop with total winding equal to the sum of the winding on all the loops. Therefore, these configurations are classified by an integer. The reasoning is quite similar to that when we were considering defects in the XY model; the difference here is that the loops are not singularities, there are no discontinuities here.

Let me point out one potential subtlety here by considering instead the case of defect free 3D nematic configurations on a sphere. We can again merge all colored loops into one, but now observe that on the sphere we can pass the sphere through the loop and thus reverse the sign of the winding. The classification is then by a nonnegative integer. The difference here is essentially that with fixed boundary conditions at infinity, the loops cannot reverse their orientation in this way. This is an illustration of what's called the action of $\pi_1(\mathbb{RP}^2)$ on $\pi_2(\mathbb{RP}^2)$ in the language of homotopy groups [Mermin, 1979; Alexander et al., 2012; Hatcher, 2002].

If we have defects, then the classification is actually fairly boring, as we can remove all closed colored loops and their color winding. First we can merge all the closed colored loops into the arcs joining the defect points. But now we can slide all of the color winding off the endpoints and make all the colored lines in the sample a single color. All that remains in the classification is the parity of the number of lines coming out of each defect point – even means no defect there, odd means there is a defect there.

The reader is encouraged to try to draw the colored curve pictures corresponding to the following operations: the changing of a "$+1/2$" disclination to a "$-1/2$" disclination, the splitting of a charge 2 skyrmion to two charge 1 skyrmions and the reversal of color winding upon bringing a skyrmion around a disclination.

2.3.1 Torus example

A rather nontrivial deformation that can be visualized with this technique is one involved in the classification of director fields on a torus. For instance, this torus could be a toroidal measuring surface surrounding a disclination loop in three dimensions. We will come back to this interpretation when we discuss 3D samples, but here we can just think of this as a question of doubly periodic 3D nematic fields in the plane.

It turns out that there are four homotopically distinct configurations on a torus which has disclination charge along one of its cycles. This means that as one runs around one of the periods of the torus, the nematic director turns in a noncontractible loop. In the 3D interpretation, the torus surrounds a disclination loop. (There are an infinite number of configurations with no such disclination charge, one for every skyrmion we place on the torus, just as in the case of the plane discussed previously). The four "homotopy classes" break into two subclasses as follows. Note that a torus has two cycles, one going around the meridian, which we have assumed here to have a disclination charge, and one going around the longitude. The longitudinal cycle may either trace out a contractible or noncontractible loop on $\mathbb{RP}^2$, depending on whether the disclination loop links an odd or even number of other disclinations. In each of these two subclasses, there are two nematic textures up to homotopy, arising from the evenness or oddness of the hedgehog charge carried by the disclination loop.

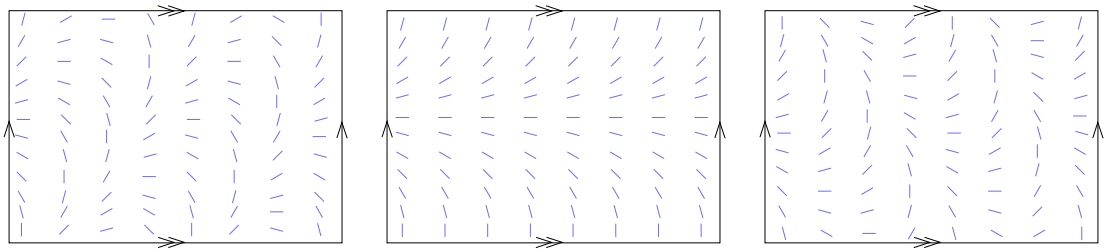

Figure 2.10: Nematic configurations on a torus with 2, 0 and -2 winding. As these are images of tori, opposite sides of each rectangle are identified, as indicated by the arrows. Note that the molecules are allowed to point in 3D, but in these configurations the molecules lie in the plane.

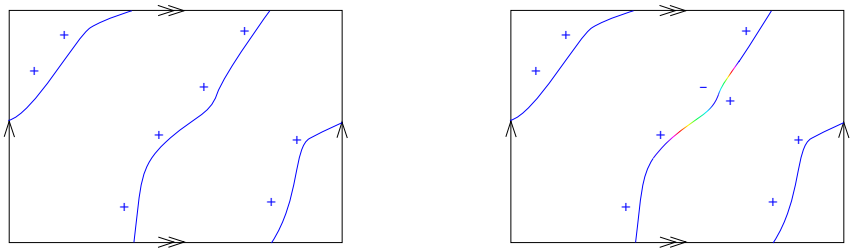

Figure 2.11: Left: colored curve picture corresponding to a configuration on a torus with 2 twists. Right: inserting a "hill" of color winding.

A priori, one might be surprised by this; in particular, let us first consider the director field on the torus where along any meridian line, the director traces out the same noncontractible loop. There is an infinite family of textures constructed by twisting this texture as we move along the longitude as in Fig. 2.10. The above classification amounts to saying that the number of twists is only well defined modulo 4, that is, there are continuous deformations from 0 twists to 4, 1 twist to -3 twists, 2 twists to -2, etc. I will show a basic homotopy between the texture with 2 twists, to the texture with 0 twists and one skyrmion which allows one to see this. It is possible to write down explicit formulas for such homotopies, but I find that these do not convey nearly as much intuition as the following sequence of pictures.

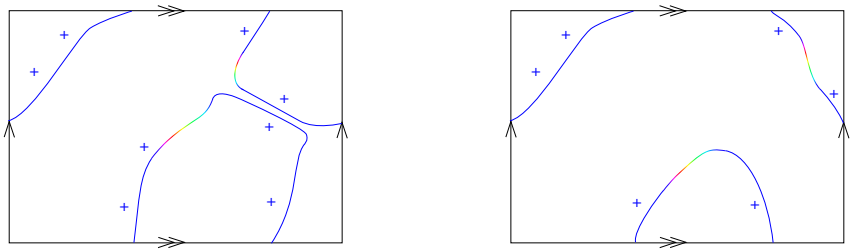

Figure 2.12: Left: After bringing two blue points until they kiss and rejoin. Right: Tightening the colored curves a bit.

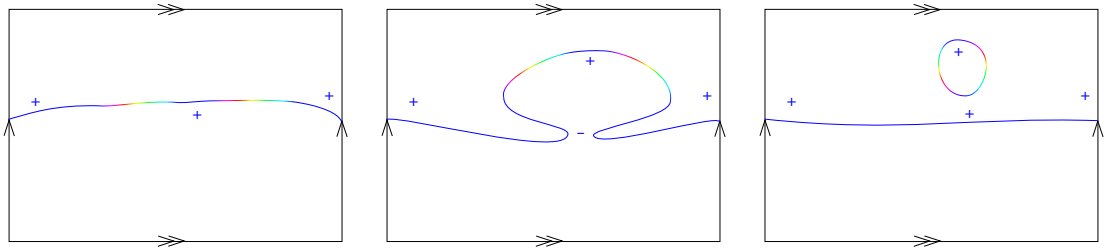

Figure 2.13: Left: Tightening the colored curves more. Center: pinching the colored curve. Right: The resulting configuration on a torus with 0 twists and one skyrmion.

First, let me draw the colored curve on the torus corresponding to a texture with 2 twists. We will choose to color points with zero y-component so that blue points will point in the x direction. Note the label of the $+$ and $-$. This is shown on the left of Fig. 2.11. Now, I choose a segment of the curve and deform the director along the color space, from blue, violet, red, orange, yellow, etc. to blue, and then reverse, from blue, green, yellow, back to blue. Physically what happens to the director is it tilts out of the xy plane through an angle of π along a curve and then back into the plane. This of course introduces no *net* color winding. The purpose of doing this is to reverse the orientation on a red segment. This is shown on the right of Fig. 2.11.

The next step is to bring this blue segment to another one and make them "kiss" and then rejoin (left of Fig. 2.12). Next, we pull the colored curve taut (right of Fig. 2.12 and left of Fig. 2.13). Now we can see that we have precisely the colored curve with zero twists, but it carries a $+2$ color winding, the signature of a $+1$ hedgehog! In fact, we can pinch off a skyrmion as in Fig. 2.13.

To get from this to a -2 winding, it's not hard to see that we can reverse the above steps and mirror them. We can then use this basic maneuver to change the twisting of any set of colored curves on the torus by 4.

Thus any configuration on a torus with disclination charge along the meridian is homotopic to one with 0, 1, 2, or 3 twists. This number of twists is a topological invariant ν which we will return to later. Let us just point out now that $\nu \mod 2$ tells us whether there is a disclination charge along the longitudinal cycle as well.

In the above, I emphasize I am not proving the classification of configurations on a torus, but rather illustrating and sharing a visualization of some aspects of it. In particular, what the inverse image and switching moves are good at is allowing us to show that certain director fields are homotopic by constructing one "with our hands". One needs to be much more careful to show that two colored curve pictures are *not* equivalent under any sequence of deformations and switching moves, or equivalently that two director fields are not homotopic. This is typically done by finding invariants which cannot change under any of the moves. By the correspondence above, these invariants are also homotopy invariants of the maps.

In Alexander et al. [2012] we find one invariant related to biaxial realizations of disclination loops which suffices to prove that these four classes are in fact distinct.

2.4 3D Nematic: 3D Sample

In a 3D sample, the colored lines become colored surfaces, and the set of allowed switching moves is also richer. I will only describe rather simple textures and manipulations in this chapter.

First, recall that the defects in a 3D sample consist of points and lines. The disclination lines are lines about which the director moves in a non-contractible loop; a cross section transverse to such a line yields a point defect in two dimensions of the type discussed previously. The point defects are sometimes called hedgehogs, due to the spiky-looking texture on a basic field $\mathbf{n} = (x/r, y/r, z/r)$. They induce skyrmion textures on measuring spheres that surround them, so that their classification is also by integers. These are classified by the behavior of a map on a measuring sphere around the point to $\mathbb{RP}^2$. I will not dwell on the classical homotopy group classification of these (leading to the calculation of $\pi_2(\mathbb{RP}^2)$), as their nature will be apparent below.

What do these defects look like when we draw in the surfaces? Disclination lines form the boundaries of the colored surfaces, just as disclination points were endpoints of the colored lines in the previous section. Therefore, there is a sheet

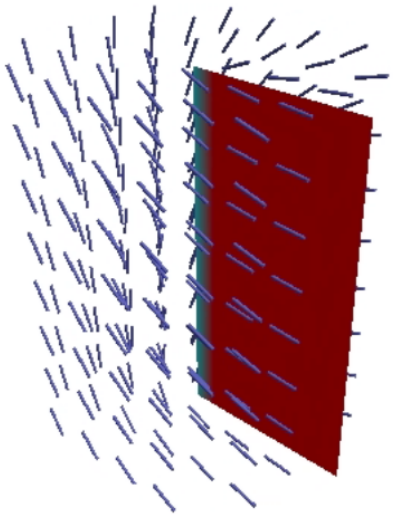

Figure 2.14: A disclination line in a 3D nematic and the colored surface coming out of it.

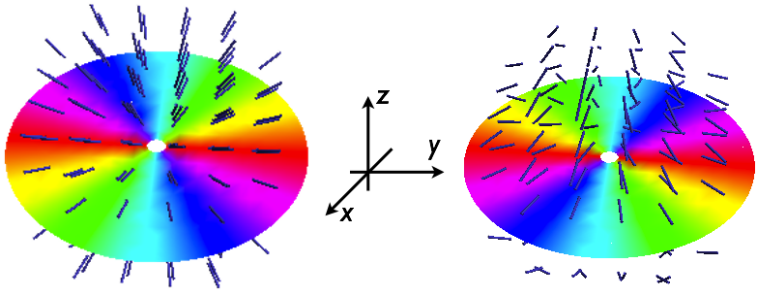

Figure 2.15: Left: radial hedgehog and colored surface. Right: hyperbolic hedgehog and colored surface.

coming out from any line defect (in general, there may be any odd number of sheets coming out of a nontrivial defect) (Fig. 2.14).

A point defect can be seen as a singular point on a colored surface where the color winding meets, i.e. a hedgehog is a color singularity on a surface (Fig. 2.15). This can be seen by considering again the radial hedgehog texture in space and noticing that on any sphere around it, there is a color winding of two – extending this into the center of the sphere, one finds a point on the surface where all the colors run into

each other. The number of the color windings and direction of the color winding relative to the winding on Fig. 2.8 determines the hedgehog charge. The homotopy between a $+1$ hedgehog and a -1 hedgehog is simply turning the singularity on the colored surface "upside down"; we described how this works in terms of the colored loops on spheres earlier, here these spheres are those surrounding the singularity.

Points and lines can interact in multiple ways. The first is that closed line defects can be viewed as point defects when they become very small. We can easily tell the difference between closed disclination loops which carry hedgehog charge and those which don't by simply counting the net color winding around the loop. Those disclination loops which carry no hedgehog charge are those which may be filled by a disk of a constant color; the disclination loop can shrink away to nothing along this disk. Conversely, hedgehogs are point-like color singularities can be viewed as punctures which might expand to circular boundaries carrying color winding, becoming disclination loops carrying nontrivial charge.

The fact that hedgehog charge creates a colored surface which extends outside away from the defect is a reflection of the fact that topological charge is conserved. If the 3D sample has a director with constant boundary conditions, then all the nontrivial color windings must be cancelled on other defects. For instance, we can imagine a pair of oppositely charged hedgehogs which form a tube pinched off at both ends. We might blow up both ends and then end up with a cylinder, which corresponds to two cancelling disclination loops. We can bring the two defects

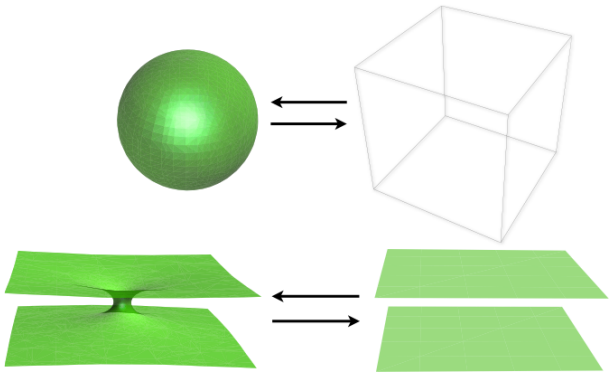

Figure 2.16: The allowed bordisms between colored surfaces – these are 3D slices of higher dimensional saddles, as in Fig. 2.6.

towards each other by shortening the length of the cylinder along its ends, and when the rings run into each other, they cancel and nothing remains.

The types of bordisms allowed between the colored surfaces are of the following two types. Closed spheres of a single color may vanish, corresponding to the change in the solution set of the equation $x^2 + y^2 + z^2 = c$ as we tune c through zero, or a tunnel can form between two sheets of the same color (provided they are locally oriented oppositely), corresponding to the change in the solution set of the equation $x^2 + y^2 - z^2 = c$ as c is tuned through zero. See Fig. 2.16 for an illustration. There are also bordisms involving defects. We have already mentioned the one which turns points into loops, and there is also one which allows disclination lines to merge. This bordism will be discussed in Section 2.7.

One nontrivial interaction between hedgehogs and disclination loops is that if we drag a hedgehog around a disclination loop, the charge on the point defect appears to change sign. It can be difficult to write down or draw the changes in a

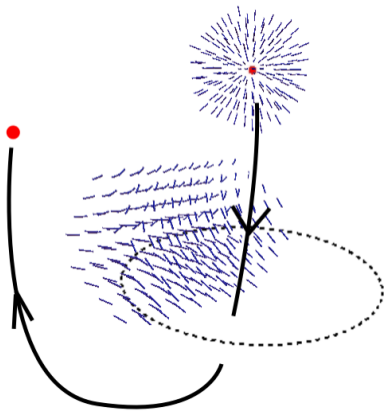

Figure 2.17: What happens at the end of the journey?

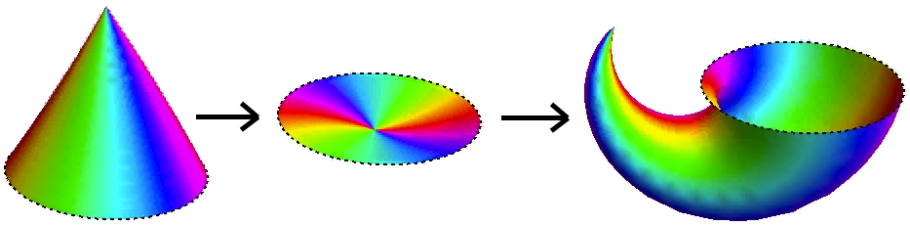

Figure 2.18: With the colored surfaces, we can see that a radial hedgehog is converted to a hyperbolic hedgehog when it is pulled through a disclination because the directionality of the color winding has reversed.

director field in a 3D sample which accomplish this (Fig. 2.17), but it is fairly easy to understand from the colored surface point of view:

The "party hat" surface on the left of Fig. 2.18 represents a disclination loop cancelling a hedgehog. Before doing anything, we see that viewed from above, the point defect carries a counter-clockwise color winding. Let us drag the point defect in a loop around the disclination, by reaching into the tip of the hat from above, grasping the tip, pulling the hat inside out, and then pulling the tip around to its original position (middle and right of Fig. 2.18).

The color winding is now clockwise, as the normal vector to the party hat has reversed, so we see here that the hedgehog charge measured on a small sphere around the tip has now apparently reversed – the local picture around the hedgehog has changed from the radial hedgehog on the left of Fig. 2.15 to the hyperbolic hedgehog on the right.

The reader may have noticed that the usual homotopy group invariants of algebraic topology usually mentioned have taken a back seat in our approach. The reason is that in order to make the correspondence etween elements of homotopy groups and regions of nematic configurations around defects, we must make additional choices. In particular, homotopy groups require a fixed point.

To see an explicit case where this matters, consider two hedgehogs in a system. If we want to combine these, it is not enough to know the winding of the colors on the

surfaces around each one, but we must also know how the surfaces are connected. In particular, they could lie on opposite ends of a cylinder whose straight lines were colored the same. Or they might lie next to each other on the same surface.

Another possibility to consider is that there could be a line disclination in the system. Then we could take two measuring spheres around the hedgehogs that passed on opposite sides of the disclination (without intersecting the defect line!) but one measuring sphere intersects the sheet coming out from the disclination and the other doesn't, leading to cancellation in one case, and non-cancellation in the other. In each case described here, computing the result with the Thom construction guarantees that one will not lose sight of the potential complications from the geometry, whereas care is required if one wishes to find the result by first reducing to manipulations in homotopy groups, then interpreting the result back in the configuration again.

2.5 Experimental visualization

Data from polarizing microscopy here is courtesy of Paul Ackerman and Ivan Smalyukh. The analysis was done jointly with Gareth Alexander.

The toron is a compact distortion that can be induced in a thin-cell cholesteric (chiral nematic) sample with homeotropic boundary conditions by shining a Laguerre-Gaussian laser beam into it. The chiral nematic cannot twist into its helical ground

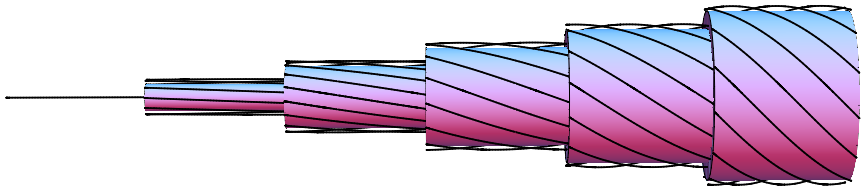

Figure 2.19: Cutaways of the nematic configuration in a double twist cylinder.

state because of the boundary conditions. A Laguerre-Gaussian beam is a beam with a phase singularity leading to a helical phase front. The laser beam allows the liquid crystal to relax into a twisted compact region called the toron. The toron was discovered by the group of Ivan Smalyukh [Smalyukh et al., 2009], and his group has been using arrays of torons to create interesting optical elements. For instance, an array of torons with a dislocation defect in the array can create a Laguerre-Gaussian mode from just an ordinary Gaussian beam.

Figure 2.1 showed a schematic reconstruction of the structure from Smalyukh et al. [2009]. The key features are the two hyperbolic hedgehog point defects above and below and a double twist ring between. Double twist is a property of chiral nematic configurations; sketched cutaways of the molecular orientation in a basic double twist tube are depicted in figure 2.19. The molecules are tangent to the center line of the cylinder and twist as one moves in the radial direction – the twisting is as one moves in the two dimensions away from the center line, hence the name.

Images were taken with multimodal nonlinear optical polarizing microscopy

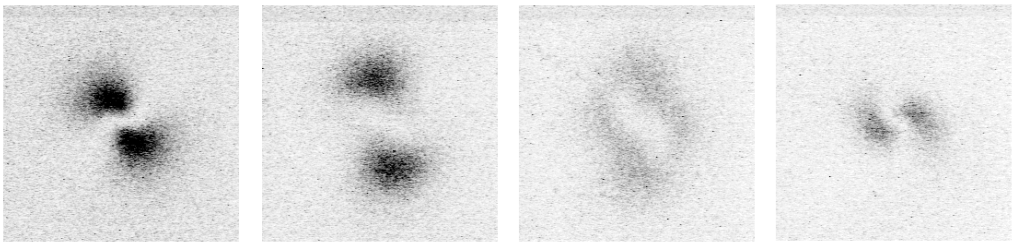

Figure 2.20: Several images from an image stack corresponding to a toron taken with MNOPM. The image width is 16 μm and images are approximately 4 μm apart in the z-direction. Darker regions indicate a higher amplitude of light polarized in the $+x$ direction.

(MNOPM) techniques [Lee et al., 2010] in particular for the images Ackerman and Smalyukh provided us, they relied on a 3-photon fluorescence process [Higgins and Luther, 2003]. Beginning with intensity data for various torons from four image stacks, polarized in 4 different angles $\pi/4$ apart in the xy plane ($E_0, E_{\pi/4}, E_{\pi/2}, E_{3\pi/4}$), Gareth Alexander and I wrote code to process the raw data and calculate the Stokes parameters:

$$I = E_0 + E_{\pi/4} + E_{\pi/2} + E_{3\pi/4} \tag{2.5.1}$$

$$Q = E_0 - E_{\pi/2} \tag{2.5.2}$$

$$U = E_{\pi/4} - E_{3\pi/4}. \tag{2.5.3}$$

Some example images are shown in Fig. 2.20. Supposing that $\mathbf{n} = [\sin\theta\cos\phi, \sin\theta\sin\phi, \cos\theta]$, and making the extreme assumption that the electric field amplitude is proportional to the electric anisotropy tensor, a short calculation shows that $I = \frac{3}{2}J\sin^4\theta$ and $\frac{Q}{U} = \tan(2\phi)$, where J is the amplitude of the signal. If we make the assumption that we can shift and normalize the calculated I from the data so that its mininum

value corresponds to 0 intensity in the xy plane and its maximum is 1, then taking the fourth root of I gives us $\sin\theta$. The shift is justified in this case as we expect that away from the toron the director is actually normal to the top and bottom surfaces, and hence the angle of the polarization from the vertical should be zero there. The angle ϕ then gives us the angle of the polarization projected to the xy plane, and we can recover a putative "director variable" $\mathbf{n}$ from θ and ϕ.

To go from this to the colored surface numerically, what we do is to reflect the director field so that it lies in the upper half of the sphere. Then we view the contour surface with n_z small and close to zero in the program Paraview [Henderson Squillacote, 2008]. Ordinarily we might just take a slice with n_z zero, but it turns out that due to the non-orientability of the line field, numerically one finds that $\mathbf{n}$ has additional branch cuts where $\mathbf{n}$ is adjacent to $-\mathbf{n}$. This procedure happens to be the simplest way to deal with such issues. A better one, though much more complicated, would be to keep track of which local coordinate system one is using for $\mathbf{n}$ at each point in the sample and take a contour that way. The downside of our approach is that what should be one surface at $n_z = 0$ is actually two nearby surfaces $n_z = \pm\epsilon$. Note that all we pick out here are the surfaces of (near) maximum I, so the fourth-root transformation we made above actually makes no difference; all we need is the fact that the regions in the data where the I is maximum correspond to regions where the molecules tend to lie in the xy plane.

In Fig. 2.21, we show the resulting reconstruction of the colored surfaces corre-

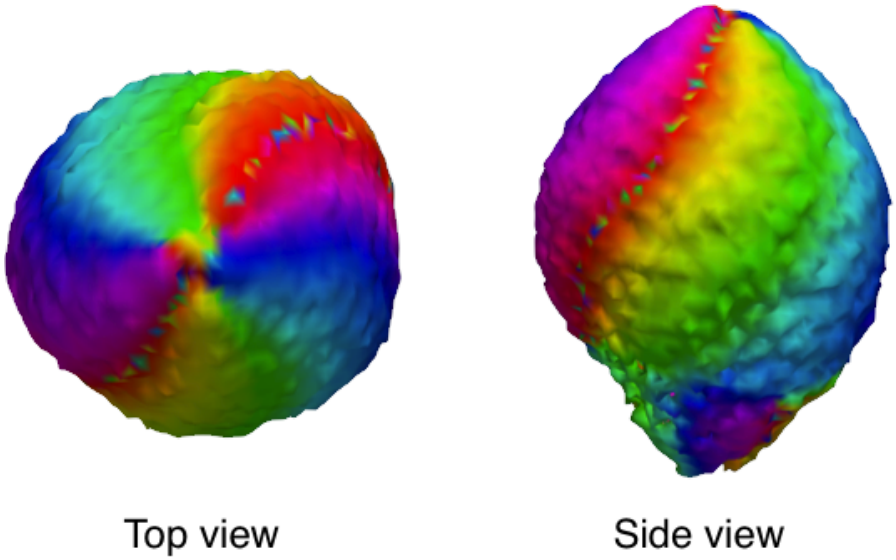

Figure 2.21: Top and side view of the colored surfaces corresponding to a toron, reconstructed from experimental data as described in the main text.

sponding to a toron. In these images and all following ones, the colored circle on $\mathbb{RP}^2$ corresponds to the circle in the xy plane, so that red points indicate molecules parallel to the x direction, and cyan points indicate molecules parallel to the y direction. The reconstructed colored surface resembles a beach ball with colors winding around it. The point defects are plainly visible at the north and south poles of the beach ball where the colors collide. The twist of the colored lines around the surface corresponds to double twist of the director. The center line of the double twist ring is the equator of the beach ball, and the diagonal slant of the colors running along longitude directions corresponds to one direction of twist, the other twist direction is the tilt through the xy plane as one moves from inside the beach ball to outside.

Despite the several assumptions in the data processing and the lack of processing

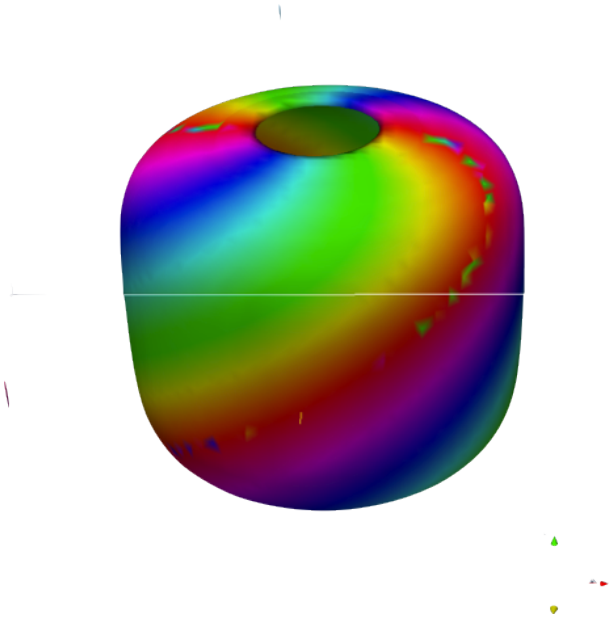

Figure 2.22: Colored surfaces corresponding to our simulation of a toron.

for noise, one can see that the resulting colored surface is relatively smooth and certainly all the key features are visible. This robustness is an advantage of these topologically defined surfaces – continuous deformations, in this case, experimental noise or distortions from the simple-minded Stokes parameter mapping, cannot change the result.

With this picture of the toron, we can now sculpt the surface to see its relation with other topological defect configurations. First, it is plain to see that it can be turned into a colored cylinder corresponding to a pair of cancelling disclination loops. In fact, Fig. 2.22 shows a simulation (more details on the simulation code are given at the start of the next section) where the defect points have blown up into rings. Indeed, Smalyukh et al. [2009] classify torons into type 1, 2, and 3 depending on whether 0, 1, or both hyperbolic point defects appear as disclination rings. The

cylinder of the surface connecting the rings, contains a full twist, due to the double twist ring.

The toron is a configuration that contains defects, but it is closely related to a nonsingular yet topologically nontrivial configuration. Suppose we bring the two disclination rings of Fig. 2.22 through the center of the beach ball and cancel them out. In order to do this, we must twist the colors again so that they line up when the rings meet. But if we do this, we end up with a torus colored along a family of diagonal Villarceau circles. To see what this means topologically, note that there are two disjoint linked circles of any color on this torus. Because they are linked, we cannot shrink this torus down to nothing without colors colliding with one another and thus introducing singularities. This is therefore a sort of three-dimensional analogue of the skyrmions we looked at earlier, and such a torus in fact is a signature of nontrivial $\pi_3(\mathbb{RP}^2)$, or Hopf charge. The classical Hopf fibration is a vector field which cannot be deformed to a constant direction despite having no singularities. The colored torus here can be seen to be a particular subset of the Hopf fibration viewed as a line field.

2.6 Simulation of colloids and blue phases

Fig. 2.23 shows simulated nematic cells from code written by Gareth Alexander. The system is a $(64)^3$ periodic grid of points with a traceless symmetric Q-tensor describ-

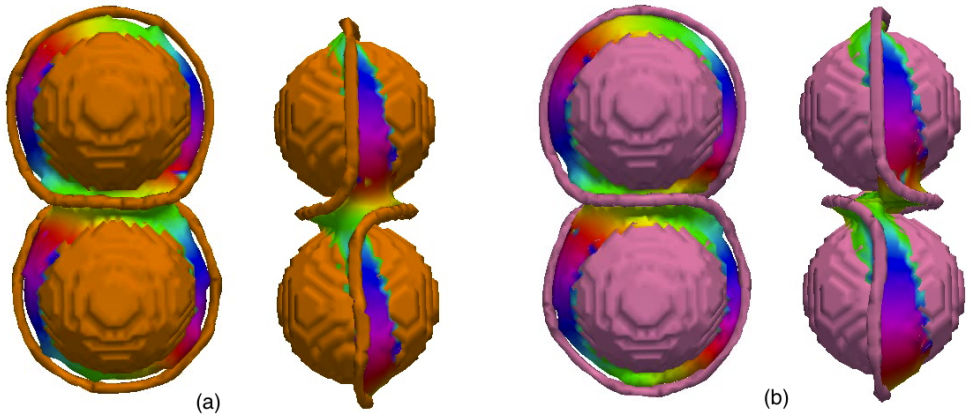

Figure 2.23: Results from simulated nematic configurations outside of two colloids with homeotropic (normal) boundary conditions. (a) Colored surfaces corresponding to a pair of Saturn rings. (b) Surfaces corresponding to a figure eight configuration of the disclination.

ing the orientational order at each point. Strong homeotropic anchoring is imposed on two boundary spheres placed at the center so that the molecular orientation is forced to point normal to the surfaces. Upon minimizing a one-constant approximation Landau-de Gennes free energy [de Gennes and Prost] from random initial conditions, sometimes two "Saturn rings" are formed about the spheres (Fig. 2.23a), and sometimes one "figure eight" ring about both spheres is formed (Fig. 2.23b). The orange and pink surfaces in Fig. 2.23 show contour surfaces at a threshold value of the order parameter. This clearly indicates the position of the disclination defects and the surface of the colloids.

What does the director field do in the bulk? Observe that the surfaces span a region between the disclinations and the colloidal boundaries. This is a reflection of the fact that the disclinations are "cancelling" the topological hedgehog charge carried by the colloidal boundary conditions. Viewed from above, the colors on the

surfaces run around the rainbow twice – this winding of the color is a reflection of the 2π angle that the director on the surface runs through and hence indicates that there is hedgehog charge.

Also, the surfaces in the case of two saturn rings and one figure 8 curve look very nearly the same, except near the rewiring site. This means that the director fields are very similar in the two samples (and certainly have the same topological behavior) except near that crossing point. It is perhaps interesting that the joined disclination loop actually carries no net topological charge: one can see that if one untwists the kink in the surface at the rewiring site, that the color winds twice one way around a colloid, then twice the other way around the other colloid. This count of color winding can be related to the self-linking numbers used by Copar and Zumer [2011] to discuss the topology and geometry of such configurations of disclinations around colloids.

The fact that the surfaces are located only close to the colloid is a consequence of the fact that the director is interesting only near the colloids – indeed, in most of the cell away from the colloids and saturn rings, the director points in a constant direction.

The next family of simulations we considered were those for blue phase textures [Wright and Mermin, 1989]. The blue phases are amazing phases of cholesteric liquid crystals which are crystalline in that they have Bragg planes, but are liquid in that they flow. As the molecules flow through the configuration, they twist and

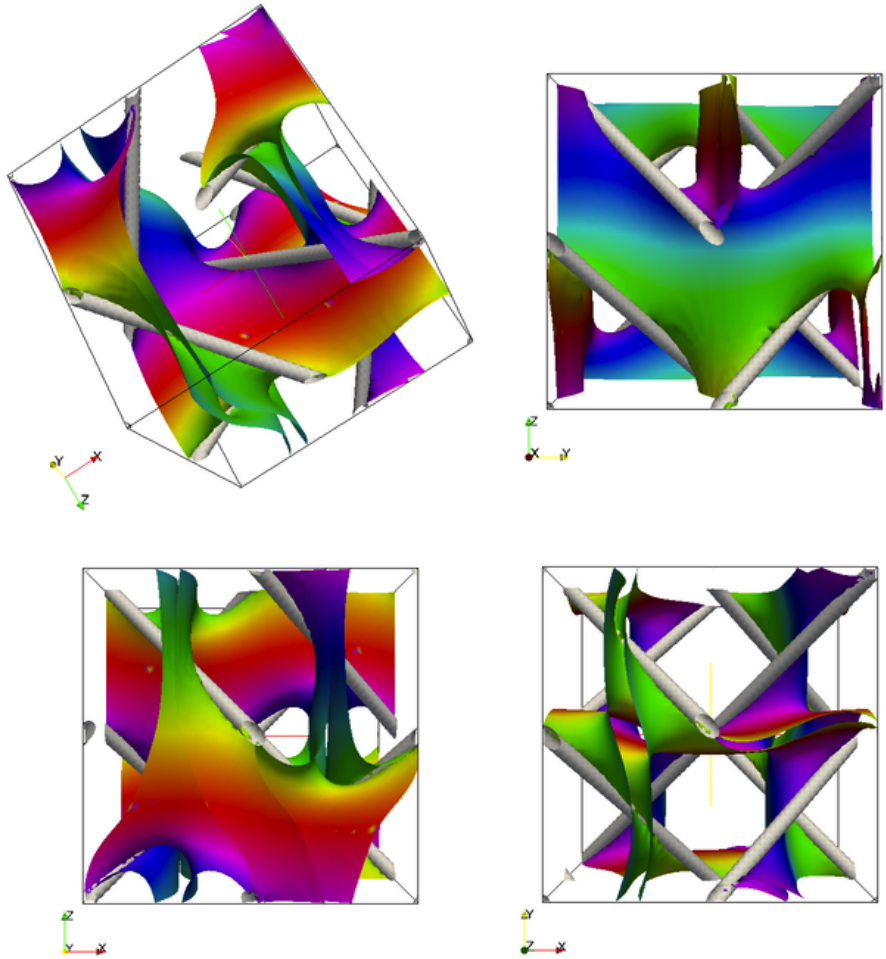

Figure 2.24: Views of the colored surfaces corresponding to a blue phase I simulation.

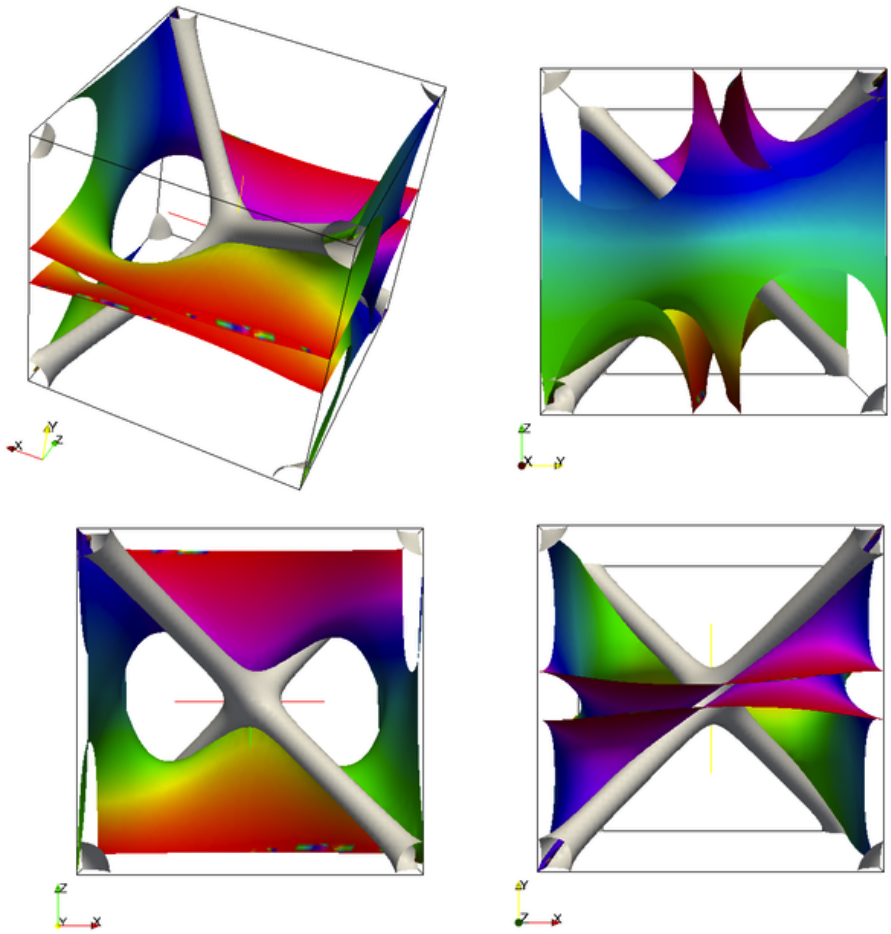

Figure 2.25: Views of the colored surfaces corresponding to a blue phase II simulation.

turn through specific directions. These phases are preferred over the helical ground state of cholesterics when saddle-splay distortions are costly.

The colored surfaces of simulated blue phase I and blue phase II are shown in Figs. 2.24 and 2.25. Observe that the sheets of the surfaces are branched over the defect networks, meaning that the sheets wind around the defect lines. In the case of blue phase I, it forms a surface resembling somewhat the cubic Archimedean screw of Elser [1996]. These blue phase structures are usually understood as packings of double twist tubes. Two of the three perpendicular families of double twist cylinders are visible in the figures as lines colored red and cyan corresponding to the directors on the center line parallel to the x and y axes, respectively. The center line of the third family is parallel to the z axis so it is only visible as the holes running from top to bottom. These surfaces are quite complex, showing the interesting relationship between defects and regions of twist. We have not yet undertaken a detailed study of the geometry and topology of these surfaces.

2.7 Measuring tori in 3D samples

I now turn to the question of classifying nematic configurations in three dimensional samples. As mentioned in the introduction, one cannot hope to classify the textures in samples with defects, as the defect sets themselves could take the form of any knot or link, and these do ot admit clean classifications. However, we can instead

take the following bordism-inspired viewpoint, after the approach of Janich [1987].

The singular set Σ of a 3D nematic configuration will consist generically of points and lines. Supposing the boundary conditions at infinity are constant (equivalently, that the system is defined on the 3-dimensional sphere S^3), these lines must close up into knots and links. We have already seen that the defect behavior around points is classified by a nonnegative integer, and also that the defect behavior on a torus around a disclination is classified by an integer mod 4. The main result of Janich [1987] is a necessary and sufficient condition on whether an assignment of charges to the points and lines in the system is consistent with a nematic configuration with defects. In this section we explicate and illustrate his result using the colored Thom surfaces and our earlier discussion of nematic configurations on tori.

Below let us assume that there is at least one disclination loop in the system. If not, then the set of defects consists only of points, and it is then clear that the sum of the hedgehog charges on these points must vanish (with the sign of the hedgehog charges now being defined by the fixed boundary conditions).

Let μ_i for $i = 1, \ldots, n$ be the defect charges assigned to the point charges (their signs won't matter below), and ν_j for $j = 1, \ldots, m$ be the charges assigned to the lines, which we orient arbitrarily. Let $Linking(j, k)$ be the (signed) linking number between two line defects. Then the set of μ_i and ν_j are consistent with a nematic

configuration if and only if, firstly

$$\nu_j \cong \sum_{k \neq j} Linking(k, j) \mod 2. \tag{2.7.1}$$

If this is true then we can define the following integer "parities" of ν_i to be $q_i = \frac{1}{2}\left(\nu_i - \sum_{k \neq j} Linking(k, j)\right) \mod 2$, we also must have

$$\sum_{j=1}^{m} q_j \cong \sum_{i=1}^{n} \mu_i \mod 2. \tag{2.7.2}$$

Before we can begin, we must say a bit more about how the ν_j are defined. Note that there are a priori many ways of mapping an embedded measuring torus in space to an abstract flattened torus like the ones we discussed earlier. The meridian line is obvious; but we must be able to choose a line on the torus which is the longitude. This is not as obvious especially if the torus happens to be knotted in a complicated way. The solution is to choose the longitude line to be one which has zero linking number with the disclination at the center of the torus. With this choice then, ν_j as we defined it earlier (the number of twists in a homotopic representative) is well-defined.

Now the first statement is transparent. As we pointed out when we defined the invariants ν, its parity mod 2 tells us whether there is a disclination charge in the longitudinal direction. But this can happen in our sample only if there are an odd number of disclination lines running through the longitudinal direction – in other

words, whether there are an odd number of defects linking this one.

The second statement is a bit trickier but we already have some intuition from our manipulations earlier. Let us first determine the meaning of the parity. Imagine for instance an unlinked and unknotted disclination loop in the sample. By the first statement, $\nu \cong 0, 2 \mod 4$. Suppose $\nu = 0$, so that $q = 0$. The configuration on the torus is homotopic to one where the line simply runs parallel to the longitudinal line. The surface in space that the disclination loop bounds is therefore just a disk of a single color. This clearly carries no hedgehog charge.

Now consider the case where $\nu = 2$ so that $q = 1$. Recall that we were able to convert two twists into a hedgehog charge. After a homotopy the configuration on a $\nu = 2$ torus can be made to be a colored line parallel to the longitude but with a color winding of two. Any sphere around this torus thus must also carry a color winding of two, and thus carry a hedgehog charge of one.

In the presence of these disclination loops, hedgehog charge is only defined mod 2, as we can always take a unit hedgehog and reverse its color winding by taking it on a loop through one of the disclination loops. However, note that by doing this, the configuration around the disclination loop picks up twists, or equivalently, color winding. The move which rids the torus of four twists is equivalent to a move ridding the torus of 2 hedgehog charge.

Therefore, q corresponds to the hedgehog charge carried by each of these tori.

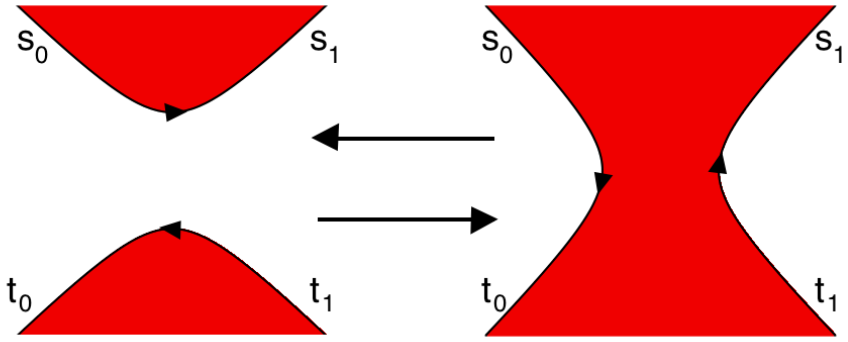

Figure 2.26: Rejoining move for disclination lines and the surfaces between them. Not shown is the local orientation around each surface which must obviously agree between the two surface pieces on the right. The labels s_0, s_1, t_0, and t_1 are longitudinal coordinates on tori around disclinations.

The second statement thus ensures that all hedgehog charge is cancelled in the system, because of the constant boundary conditions at infinity.

We can easily check the second statement for the case of a single unknotted line defect in the system. When $\nu \cong 0 \mod 4$, the line defect itself contributes even hedgehog charge. In order for there to be no hedgehog charge at infinity, $M = \sum_{i=1}^{n} \mu_i$ must be even, since hedgehog charge can only be reduced mod 2. The same reasoning holds for $\nu \cong 2 \mod 4$, except here the line defect contributes an odd amount and therefore we must have M odd.

Conversely, suppose that the total charge from the hedgehogs M is even and that $\nu \cong 0 \mod 4$. This condition on ν is consistent with a texture on the torus which has a color winding of M, and it's not hard to draw a continuous surface joining the line to the hedgehogs. The same thing works in the case of M odd, as well.

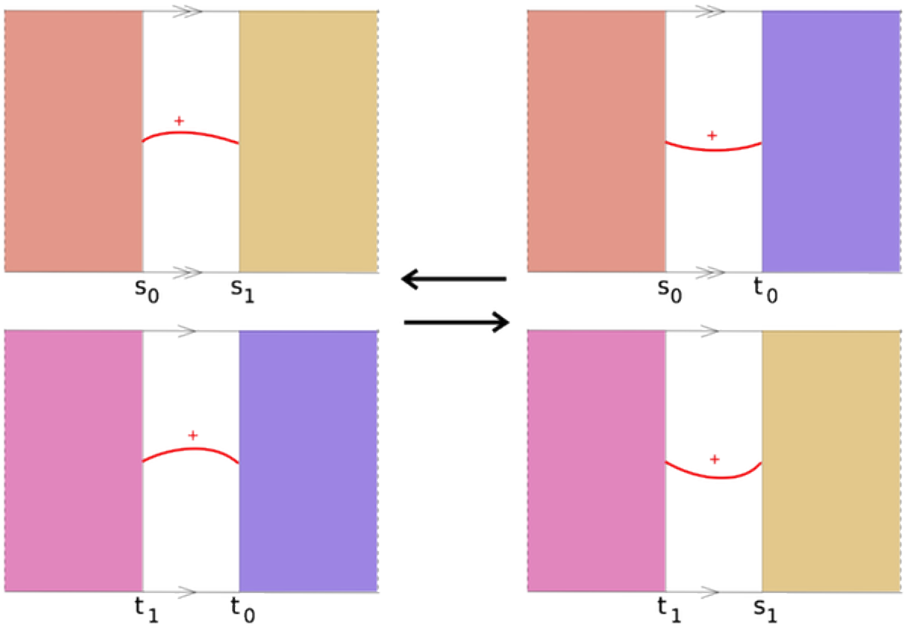

Figure 2.27: The effect of the rejoining move for disclination lines on the measuring tori surrounding the disclinations. The labels s_0, s_1, t_0, and t_1 are as in Fig. 2.26.

To prove the second statement for all sets of line defects, we just need to check that the sum of parities of line defects is conserved when we merge line defects as in Fig. 2.26, as all arbitrarily knotted and linked line defects can be generated from a single unknotted one by such rejoining moves. This follows from the following picture of what actually happens in such a rejoining move.

This rejoining is a bordism of defects, with an associated bordism of colored surfaces. In order for this to be possible, the surfaces must be colored the same and oriented the same way in a neighborhood of this move. Thus when rejoining two arcs, the pictures on the tori T^2_α and T^2_β surrounding each one initially look like those on the left of Fig. 2.27. After the move s_0 is joined to t_0, and s_1 is joined to t_1. By the definition of ν as the number of twists, it's clear that sum of the twists in

the new disclination loop configuration must be equal to what it was before, as the change we made was local and did not reverse the orientation around the colored loops.

This result shows that despite the problem of classifying nematic configurations with defects being rather difficult, it still admits a discrete type of classification; the idea of reducing a very complicated defect set to a simpler one also turns out to be profitable here.

2.8 Abstract formalism

The Pontryagin-Thom construction in the form I've used it is explained in Chapter 20 of tom Dieck [2008] (for a more relaxed exposition of the special case of maps to spheres, see Milnor [1965]). The precise statement is as follows:

Let ξ be a real vector bundle over a manifold B. Homotopy classes of maps from a manifold M to the space $X = \xi \cup \{pt\}$ are in one-to-one correspondence with bordism classes of ξ-submanifolds of M. To go from a generic map $f : M \to X$ to a ξ-submanifold, take the inverse image $f^{-1}(B)$. To go from a ξ-submanifold S to a continuous map, we map ξ to the normal bundle of S, νS, and then map pt to the complement $M \setminus \nu S$.

A ξ-submanifold S of M is a submanifold of M with a bundle map from its

normal bundle to ξ (so that points of S are mapped to B). This is sometimes called a framed submanifold in the case that ξ is a trivial bundle over a point (i.e. a vector space).

The examples of the 2D and 3D nematics fit into this jargon in the following way: with the order parameter space $\mathbb{RP}^1$ of the 2D nematic, the bundle ξ was simply the open interval $\mathbb{RP}^1 \setminus \{\leftrightarrow\}$, naturally a line bundle over a single point. For the space $\mathbb{RP}^2$ of the 3D nematics, ξ was the Mobius strip identified earlier, which is a line bundle over the equator.

As a side note, the Pontryagin-Thom construction for maps to S^2 was applied by Teo and Kane [2010] to study hedgehog defects at interfaces between topological insulators and superconductors. The version for maps to S^2 can also be used to study and classify triply periodic vector fields (and indeed was the first case that I learned) [Deturck et al., 2011].

One barrier to applying the above formalism is the fact that the target space must be the one point compactification of a real vector bundle ξ, but though spheres and real projective spaces have this structure, most spaces do not. However, we may extend this way of thinking by noticing that what we are primarily doing is peeling away the highest-dimensional chunk of the target space. For example, note that in the backwards construction from directed lines or colored surfaces back to a 2D or 3D configuration, most of the sample gets assigned a constant value, and the rest of the distortion in the configuration is squeezed into neighborhoods of

the Thom surfaces. Therefore for a general target space X with a decomposition into pieces with different dimensions (e.g. one with a CW structure or other cell decomposition [Hatcher, 2002]), intuitively, most of the domain is mapped into the piece of the target space with maximal dimension, so we ought to look at the inverse image of the space X' that remains after removing those and then keep track of the data in a neighborhood of that. In favorable circumstances, X' has no singularities and is a manifold, then the theorem above holds. I believe a quite general version of Pontryagin-Thom which applies to all X' is proved in Buoncristiano et al. [1976], but I have not fully digested it. If X' has singularities (e.g. places where lower dimensional pieces intersect) then we should expect similar singularities in the inverse image.

Instead, let me discuss a partial example, biaxial nematics or cholesterics, where the relevant order parameter space is a three-dimensional quotient of the rotation group by the symmetries of a rectangular prism, called $SO(3)/D_2$ [Mermin, 1979]. Equivalently, this is a quotient of the three-sphere S^3 by the group of quaternions Q_8. One concrete construction of this space is by taking a cube and identifying opposite faces with a quarter twist. We show in Fig. 2.28 a stereographic projection of a tiling of S^3 by 8 curved cubes (note that the faces of the cubes are spherical and the dihedral angles between the faces of these cubes are $2\pi/3$ due to the positive curvature); the cube in the center is a fundamental domain for this identification and we could in principle write down equations defining its faces – these would be equations of great 2-spheres in the 3-sphere (analogous to great circles on the

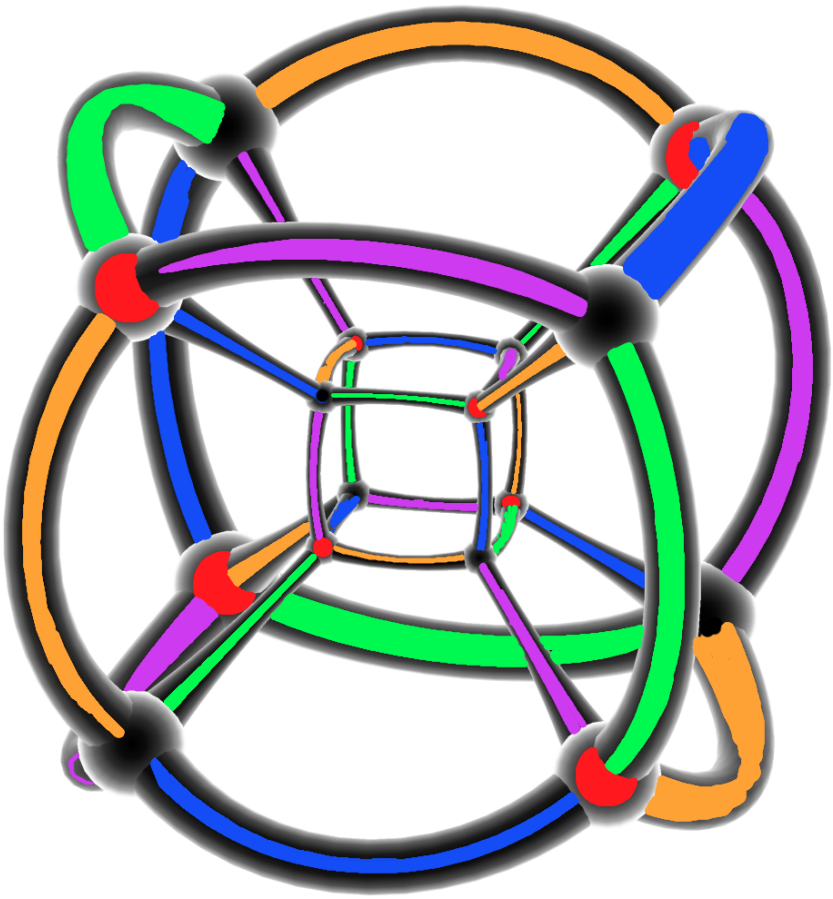

Figure 2.28: A tiling of the 3-sphere S^3 by eight curved cubes, where the tiling group permuting the tiles is the group of quaternions. Each cube is identified with its neighbors after a quarter-twist along the axis of translation. The sets of the vertices and edges which are so identified (the group orbits) are colored. Note that there are two classes of vertices (red, black), and four classes of edges (green, blue, orange, purple). There are also 3 families of faces (not colored), which can be identified from the distinct cyclic ordering of edges and vertices around each. As a start, note that opposite faces are always identified. The figure was edited from an image generated with the software Jenn3D [Obermeyer, 2006].

2-sphere) which intersect at angles of $2\pi/3$.

Under the identification under quarter twists, this solid cube becomes a complex with two vertices, four edges, three faces, and one three-dimensional cell (the interior of the cube). In Fig. 2.28, the vertices and edges which become identified are depicted by their color. See the caption for more details. This space was among several discussed by Poincaré in his seminal paper Analysis Situs [Volkert, 2011; Poincaré, 2010].

Following the above philosophy, we should consider the inverse image of the 2-dimensional skeleton of this complex (the union of the vertices, edges and faces), and this will generically be a singular codimension one complex in the sample. The edges where the three faces of the cube intersect will correspond similarly to edges in the inverse image, and there will also be vertices where the four edges intersect. Thus the inverse image surfaces for biaxials will look foam-like, with 3 faces meeting in edges and 4 edges meeting in vertices. This is evident already in Fig. 2.28 which could be regarded as showing the inverse image construction for the quotient map $S^3 \to S^3/Q_8$.

As biaxial nematics only admit line defects of various sorts [Mermin, 1979; Alexander et al., 2012], in a general configuration, we will see the faces of these inverse image "foams" connecting various defect boundaries and junctions.

From simulation data, one could calculate the value of the biaxial order parame-

ter as a particular 3 by 3 rotation matrix at a point in the sample which diagonalizes the Q-tensor there. In order to look at this as a point in the cube illustrated above, it would probably be most convenient to write the rotation in terms of quaternions or points on the unit 3-sphere in 4-space, and then identify whether it lies on the faces of the cube described above using explicit equations. It is not immediately clear to me what the relationship to maps to $\mathbb{RP}^2$ gotten by looking at just the long axis would be, though, in particular, whether the colored surfaces defined earlier are related in a clear way to the foam-like inverse image complexes here.

2.9 Summary and Outlook

Though some of the descriptions and definitions above may have seemed complicated, this is still much simpler than attempting to visualize deformations of a line field in a 3D sample. Furthermore, defining the surfaces and computing them is simply a matter of having one's visualization software compute and color isosurfaces corresponding to some projection of the director. Indeed, before I began playing with these pictures, I had no idea that such a detailed representation of the topology was possible. New questions come to mind which could not have even been imagined before.

Looking forward, several natural questions come to mind. First, it would be interesting to see more explicitly some examples of this construction applied to

systems with other order parameters, along the lines of the discussion in the previous section. Next, to what extent can these surfaces be used to estimate the energy of a configuration? Certainly once we have gone to the surface description we have lost a lot of information, but the surfaces still have the property that they track where the orientation is changing. Finally, the question arises as to whether the surfaces might be used to understand at least qualitatively the propagation of polarized light through nematic samples. Intuitively, regions with no surface have molecules roughly oriented in the same direction, so perhaps one can look for holes in the surfaces through which light polarized in that direction can propagate easily.

Chapter 3

Smectics and Broken Translational Symmetry

In this chapter I consider problems relating to defects in systems with broken translational symmetry. The first two sections are an adaptation of my 2009 paper with Alexander and Kamien [Chen et al., 2009]. The first section reviews difficulties with a "naïve generalization" of a homotopy theory treatment of defects in smectics and directed smectics and points out the missing piece in that argument. In short, the naïve generalization assumes an independence of orientational order and translational order which is not justified. Orientations in such systems are derived quantities, arising from gradients of the translational phase variables.

The next section describes a surface model for 2D directed smectics and smectics

which allows for an intuitive understanding of the defect behavior without too much mathematics.

The remaining sections elaborate on some unfamiliar mathematical objects which one is led to from the considerations in the previous two sections. Section 3.3 returns to an idea introduced in section 1 which is that orientational order in crystalline systems is determined by the components of the gradient of the phase variable. Thus we build a space over the sample space with extra coordinates that keep track of the phase and the components of its gradient. There are compatibility conditions between the phase and its gradient which result in certain "preferred" planes that potential measuring paths in the sample must be tangent to. These planes are a basic example of a contact structure.

Section 3.4 discusses in greater detail the reflection symmetry of smectics and the orbifold structure of its space of order parameters, which we will first see in section 3.2. In short, the phase ϕ lives on a circle with a mirror plane due to the $\phi \to -\phi$ symmetry. This space $S^1/\mathbb{Z}_2$ (not to be confused with $\mathbb{RP}^1$) has two distinguished mirror points at $\phi = 0, \pi$ which turn out to be significant for possible defects. The phase spaces of smectics and crystals are crystallographic orbifolds, which are spaces with singularities one gets when taking the quotient of Euclidean space (for smectics, the real line) by a crystallographic group of isometries. This group is associated with a tiling of space with compact tiles, which can be viewed as copies of the orbifold. These tiles may contain points which are fixed by some of

the crystallographic group elements (in particular by the rotations and reflections); these fixed points turn out to be the orbifold singularities. The goal of this section will be to point out that these singularities (which are a bit like cone points in the order parameter space) allow smectics and crystals to have defects which are not points of discontinuity, but merely points of non-smoothness.

Finally we conclude by bringing together the open questions suggested by this work.

Let me end this introductory section with a brief philosophical comment. In some sense, the thrust of this chapter is the reverse of that of the previous one. In chapter 2, we began with nematic configurations which are usually studied as three-dimensional orientational fields and used the Pontryagin-Thom configurations to reduce the information to a set of surfaces. In this chapter, we will discuss smectics and crystals, which are typically understood in terms of simply the positions of the layers and sites of the atoms. What we will clarify is what the sample is doing "in-between" these layers; we will spend a bit of effort understanding what order parameter space the sample is mapped to.

3.1 Defects, fundamental groups and Goldstone modes

Systems with broken symmetries are described by non-vanishing order parameters. When the symmetry is continuous there is a degeneracy of ground states continu-

ously connected by the underlying symmetry. Each of these equivalent but different ground states is represented by a different value of the order parameter. The order parameter field is a local measure of the system's order; in other words, each configuration of a medium defines a map from physical space (the plane, in this paper) to the set of order parameters. The goal of the topological theory of defects is to classify the defect structures in physical media by analyzing the properties of these maps which are invariant under continuous deformation, or homotopy.

Recall the XY model of two-dimensional spins on the plane, discussed in the first chapter. In the broken symmetry state the spins align along a common direction, making an angle θ with the $+\hat{x}$ direction. The ground state corresponds to a constant value of θ and the ground state manifold is thus the unit circle, S^1. Locally, the orientation at a point P in any texture corresponds to some point in the ground state manifold and we can think of the ordered state as a map from points in the sample to directions given by points in S^1. Upon traversing a closed loop in the sample the orientation must return to its initial value so that θ can only change by an integer multiple of 2π, known as the degree, or winding number. A non-zero winding indicates that the loop encircles a topological defect, or vortex, whose strength is given by the winding number. Thus, defect states of the two-dimensional XY model are characterized by a single integer.

These notions are formalized in the homotopy theory of topological defects [Mermin, 1979; Michel, 1980; Trebin, 1982]. There we start with two groups, G and H,

which are the symmetry groups of the system in a disordered and ordered state, respectively, so $H \subset G$. The ground state manifold is the quotient space G/H and the topological defects are classified by the conjugacy classes of the fundamental group, $\pi_1(G/H)$ [1]. For systems without broken translational symmetry, the ground state manifold can usually be identified with the order parameter space, as the ground states consist of constant maps to the latter. In the XY model the disordered state has full rotational symmetry, so $G = SO(2)$, which the ordered state breaks completely, so H is the trivial group. The ground state manifold is $G/H \cong S^1$, the unit circle, and the fundamental group is $\pi_1(S^1) = \mathbb{Z}$, reproducing our intuitive result. Two-dimensional nematics are almost identical, except that, since nematics have no heads or tails, we must identify θ and $\theta + \pi$, so that now $H = \mathbb{Z}_2$. We then have $G/H = \mathbb{R}P^1$ and $\pi_1(\mathbb{R}P^1) = \frac{1}{2}\mathbb{Z}$, giving the familiar Frank indexing of nematic disclinations [Frank, 1958]. In this way, the topological theory provides a general framework for the classification of defects (at least up to the behavior on spheres around them) in any broken symmetry ordered medium. Amongst the key insights it affords is that products of loops in the fundamental group yield information on how defects combine or split and, particularly, the path dependence of these processes when the fundamental group is non-Abelian [Poénaru and Toulouse, 1977].

Now I describe the "naïve generalization" [Mermin, 1979], to systems with bro-

[1] I have not defined the fundamental group of a space X in this dissertation, but it is the group formed by concatenating closed loops in X (with a fixed base point) and considering them up to homotopy. For mathematical details see Hatcher [2002].

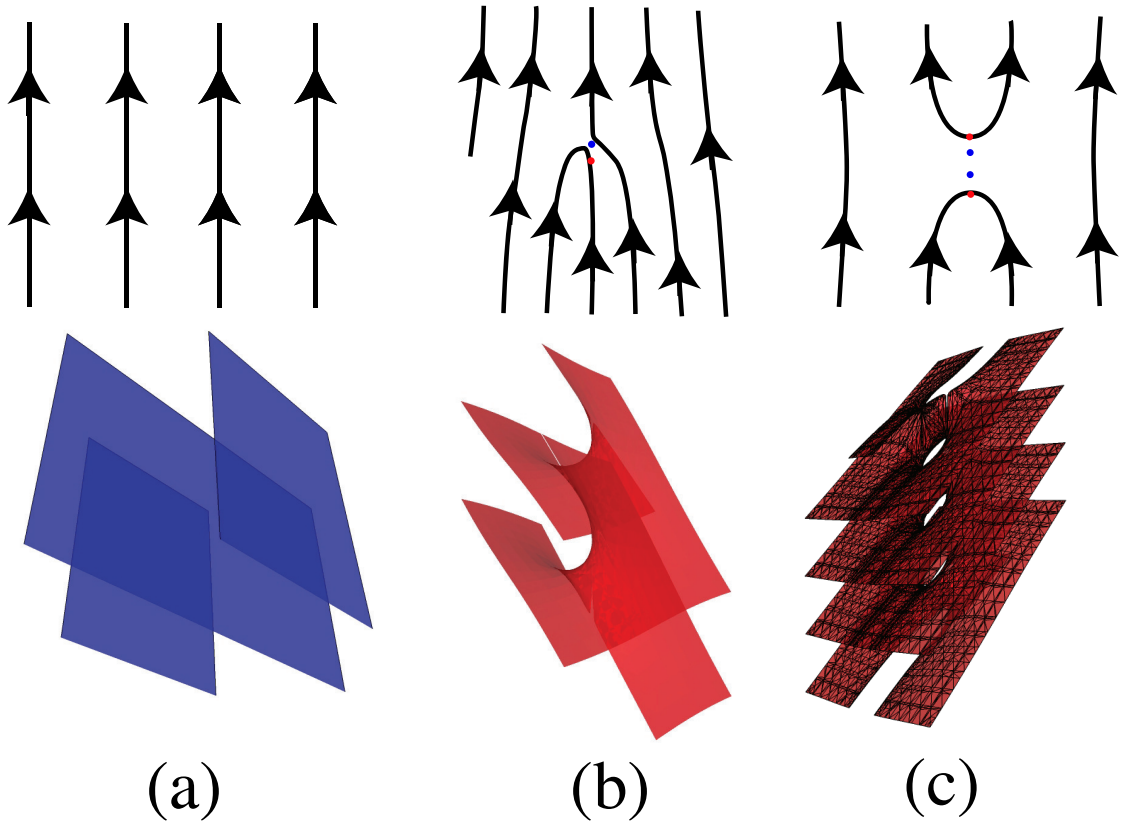

Figure 3.1: Directed smectics in the plane. The top row shows the layers derived from slicing the surface shown in the bottom row at integer values of the height, *i.e.* taking level sets. Red dots indicate the positions of branch points and blue dots indicate the positions of -1 index critical points (saddle point). (a) ground state (b) dislocation / helicoid, (c) two dislocations, note the cylindrical "hole" puncturing the planes, reminiscent of Riemann's minimal surface.

ken translational symmetry, such as directed lines in the plane and two-dimensional smectics. Keep in mind that these results will be reconsidered later. In the directed smectic model, one ground state consists of parallel layers, perpendicular to $\hat{x}$ and with equal spacing a and a well-defined orientation as in Figure 3.1(a). The symmetries of the ground state consist of a translation of the layers by a in the $\hat{x}$ direction, arbitrary translations in the $\hat{y}$ direction, and rotations by 2π of the system. Thus we might take G to be the two-dimensional Euclidean group consisting of two translations and a rotation, $H = \mathbb{R} \times \mathbb{Z}$ so $G/H = S^1 \times S^1 = T^2$, the two-torus, where the first factor is translations *modulo* a and the second is rotations *modulo* 2π. Coordinates on the ground state manifold are naturally provided by the phase ϕ (acted upon by translations) and the direction θ of the layer normal (acted upon by rotations). ϕ is the spatially-varying phase variable describing the density of the layers. If we consider homotopy classes of loops with non-zero winding only in the ϕ direction we recover dislocations. In particular, the usual construction for the Burgers vector via counting layers is equivalent to looking at the winding number of ϕ, since we draw a new layer for every multiple of a in ϕ. The fundamental group of the torus is $\mathbb{Z} \times \mathbb{Z}$, so in this generalization, defects in the full system should be characterized by pairs of integers (m, n), m corresponding to dislocation charge and n corresponding to disclination charge.

In the case of the smectic, the ground state is again a set of parallel lines perpendicular to $\hat{x}$, but without orientation. Therefore, the symmetries include translation by a in the $\hat{x}$ direction, and rotations by π owing to the nematic-like symmetry.

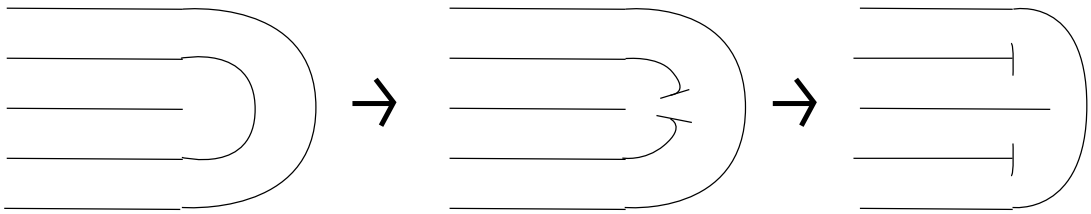

Figure 3.2: The generation of a dislocation pair in the presence of a $+1/2$ disclination.

A rotation by π followed by a translation by δ is equivalent to translation by $-\delta$, which leads to a twist in the order parameter space. Again with ϕ, θ being the coordinates of the ground state manifold, we must now identify ϕ with $-\phi$ when $\theta \to \theta + \pi$. The order parameter space is no longer the two-torus, but is the Klein bottle. To construct the fundamental group of the Klein bottle we start with the free group of two elements S, representing a shift by a, and F, a rotation or flip by π. Note, however, that $FS^{-1}F^{-1} = S$ and it follows that the fundamental group is $\langle S, F | FSF^{-1}S = e \rangle$, where e is the group identity. This group is the semidirect product $\mathbb{Z} \rtimes \mathbb{Z}$ [2], so one might classify loops by two numbers (m, n), where m counts the number of dislocations and n counts the number of disclinations. Algebraically, one can show that if n is odd, (m, n) is conjugate to $(m + 2, n)$, *i.e.* $S^{-1}(FS^m)S = FS^{m+2}$. This can be interpreted graphically and elegantly as the generation of a dislocation pair in the presence of a $+1/2$ disclination, as in Figure 3.2, after Figure 3 of Kurik and Lavrentovich [1988].

Though the algebraic structure we have presented is a natural generalization of

[2] In Chen et al. [2009], we mistakenly wrote $\mathbb{Z} \rtimes \mathbb{Z}_2$, the group arising from this construction for a *three-dimensional* smectic.

the standard study of topological defects [Kléman and Michel, 1978; Kléman and Lavrentovich, 2003], it fails to correctly characterize the defects of either system. Mermin recognized this in Mermin [1979] and pointed out the difficulty of using the standard approach when translational symmetry is broken. The attentive reader may already have noticed several differences between these two systems and the XY model. First, the ground state manifold in these two cases is not the same as the order parameter space. In both cases, the order parameter space is the one-dimensional set of possible phase values, but the manifold of ground states is a two-dimensional set, with the extra dimension being an angle. Furthermore, homotopy theory predicts entire classes of defects that are not present in the physical system. Poénaru proved that directed line and smectic models cannot have disclinations with index greater than +1 [Poénaru, 1981], and yet they are predicted by the homotopy theory. More generally, the problem lies in the allowed changes of the points in G/H as one moves along a path in the sample. For a system with liquid-like order, such as the nematic, any variation in the G/H parameter can be accommodated, *i.e.* any path in the ground state manifold can be mapped onto the specified path in the sample. However, the same is not true for translationally ordered media, like the smectic.

In fact, as is obvious in hindsight, we cannot consider the coordinates ϕ, θ of a point in the ground state manifold as independent variables. Recall that they arise from the order parameter $\phi(\mathbf{x})$, the former as its value at a point and the latter as the direction of its gradient.

In order to identify the position in the ground state manifold of a configuration at any point P, we must consider the Taylor series for the configuration $\phi(P+\mathbf{x}) \approx \phi(P) + \nabla\phi|_{\mathbf{x}=P} \cdot \mathbf{x} + \cdots$ [3]. The ground states of the directed line and smectic systems are linear functions $\phi_{\phi_0,\mathbf{k}}(\mathbf{x}) = \phi_0 + \mathbf{k}\cdot\mathbf{x}$, where $\mathbf{k}$ is a unit vector. We assign the ϕ component of the local ground state to be ϕ_0, as usual, and use the directionality of $\nabla\phi|_{\mathbf{x}=P}$ to set the second component, $\mathbf{k}$. Note how this generalizes the usual procedure which works for liquid-like systems with no translational symmetry breaking, where the ground state is simply a constant. If the ground state has structure up to order n, strictly speaking, we should keep data at every point of the configuration also up to order n.

There is an immediate implication regarding the smoothness of the phase field at defects as well. When ϕ has a nontrivial winding about a single point (i.e. there is a dislocation), we know it must be discontinuous there. Suppose though that a loop has nontrivial winding in $\nabla\phi/|\nabla\phi|$. In this case the unit normal must be discontinuous, but this only implies that $\nabla\phi$ is discontinuous or zero. It follows that at a disclination ϕ is either singular or critical (in the sense of having zero derivative).

Returning to the question of realizability of paths in the order parameter space, note that there is no issue if we only keep the behavior of ϕ; restrictions only appear when we try to impose both ϕ and its gradient. More explicitly, given $\phi(\gamma(s))$ and

[3] Here and throughout ∇ acts on the two-dimensional xy-plane.

$\nabla\phi(\gamma(s))$ on a path $\gamma : [0,1] \to D$ in our domain D, we must have

$$\frac{d\phi}{ds} = \nabla\phi \cdot \dot{\gamma}, \tag{3.1.1}$$

where $\dot{\gamma}$ is the tangent vector to γ. This condition for realizability on a path is just the definition of gradient, but we shall see in section 3.3 that the geometric consequences on possible ϕ and $\nabla\phi$ that we might impose on the sample are quite subtle.

As a result, although the smectic breaks both rotational and translational symmetry, it has only one Goldstone mode, equivalent to the Eulerian displacement field $u(\mathbf{x})$. Only the paths in the ground state manifold which correspond to this mode can be realized as long-wavelength distortions from the ground state. The reduction in the number of Goldstone modes and associated restriction of the realizable paths in systems of broken translational symmetry arises because the rotational and translational degrees of freedom are coupled into a composite object [Toner and Nelson, 1981; Sethna and Huang, 1992; Low and Manohar, 2002], in a manner akin to the Higgs mechanism for gauge fields [4]. Only when the number of Goldstone modes is equal to the dimensionality of the ground state manifold do we have sufficient freedom to be able to match any path in the ground state manifold to any path in the sample, as is required for the application of the standard homotopy theory. Here we have only the freedom to match paths in the order parameter space.

[4] The astute reader might wonder about the restriction of paths for a spontaneously broken gauge theory where the Goldstone mode is also absent. There are no restrictions: in the gauged case the winding is not a non-trivial loop in a ground state manifold connecting equivalent but distinct ground states, but rather a winding on a gauge orbit connecting different representations of the same physical state.

Of course, since any configuration can still be identified locally with a point in the ground state manifold, the defects that do occur will still correspond to non-trivial loops in G/H and we can continue to label them by the winding numbers of these loops. However, the possible defects that can arise (i.e. those consistent with the realizability condition Eq. 3.1.1) should be determined from the homotopy of $\phi(\mathbf{x})$ and $\nabla\phi(\mathbf{x})$ together, and not from the structure of the ground state manifold.

3.2 Surface model

In this section, we look at directed smectic and smectic configurations from a different point of view. Rather than try to artificially choose ϕ and $\mathbf{p}$ and then try to get $\mathbf{p}$ to be equal to $\nabla\phi$ along some path, we will simply work with the phase function ϕ and see what can be said about it and its defects directly. Since the smectic is represented by level sets of a phase field on $\mathbb{R}^2$, we may visualize the phase field as a graph of a surface in a three dimensional space where the third dimension is the values of the phase. From this perspective it becomes possible to sidestep the difficulties that we have discussed and to understand, for instance, Poénaru's rigorous result afresh. We begin with the simpler case of directed smectics.

Starting with a ground state for the lines, $\phi = \phi_0 + \mathbf{k}\cdot\mathbf{x}$ is the equation for a plane and defines a line for fixed values of ϕ. Taking level cuts at $\phi = na$, $n \in \mathbb{Z}$ we find lines in the xy-plane, with uniform spacing, a. The $\phi \to \phi + a$ symmetry implied

by the phase field construction of the layers means that instead of one plane, we have an infinite stack of equivalent planes each one shifted along the ϕ direction by a multiple of a as shown in Figure 3.1(a). Because of this, we can instead take a cut through all the planes at $\phi = 0$, for instance, and equivalently generate the ground state viewing ϕ as an element of S^1. This multiplane description is natural from the point of view of defects, as encircling a defect signals that a locally single-valued function (here, which plane you are on) becomes multivalued. Thus, dislocations connect the different sheets together consistent with their charge. For instance, when taking a Burgers circuit around a +2 dislocation, we know that ϕ changes by $2a$. This means that the sheets must be connected together with the topology of a helicoid so that dislocations may be thought of as branch points as shown in Figure 3.1(b). Multiple dislocations are given by surfaces connected by multiple helicoids, *e.g.* Figure 3.1(c). This approach has been usefully employed to visualize dislocations in waves [Berry, 1981][5] and we extend it to incorporate disclinations. Disclinations, as we have discussed, are either zeroes or singularities of $\nabla\phi$ and so in this height model, the disclinations correspond to critical points or cusps in the surface [Trebin, 1982]. For instance, a "mountain" or "trough" in the height function is a +1 disclination and the disclination sits at the peak or nadir. Concretely, an equally spaced, +1 disclination is represented by a regular cone $\phi = |\mathbf{x}|$, the level sets at $\phi = na$ giving circular layers with equal spacing, a. Similarly, negative charge disclinations correspond to saddles on creatures with

[5] Note that although the branch point of a helicoid is quite apparent when viewed in three dimensions, in any given slice of it, the branch point is not apparent since the layers all remain smooth, see particularly, images in Nye and Berry [1974].

varying numbers of appendages. Interestingly, the core of the helicoid also carries a +1 disclination charge, since the layers from 0 to na intersect in the core with a pattern like radial lines, the gradient $\nabla\phi$ being perpendicular to the layers must also make a full turn. If the layers become flat far away from the helicoid core, this implies the existence of a -1 disclination. And indeed, these are visible in the surface model (highlighted in Figure 1).

The notion of topological equivalence in this model is intuitive. First, note that deformations of these surfaces (with the restriction that points with horizontal or vertical tangent planes are singular) correspond to the class of allowed paths in the $\phi, \nabla\phi$ space that we discussed in the previous section [6]. Hence, results from Morse theory and singularity theory on the topology of such branched surfaces and their defects may be regarded as global consequences of the local restrictions developed earlier. As an example, consider Poénaru's result on the lack of disclinations of charge higher than +1. In our approach, Poénaru's result becomes transparent: two +1 disclinations cannot join because the peaks of two mountains cannot merge on a surface without a mountain pass between them interfering at some point. A mountain pass has a critical point with the geometry of a saddle, and the contours of constant height draw out a -1 disclination in the two-dimensional line system. Similar arguments hold for two troughs and even for a trough and a mountain.

Smectics can also have 1/2 disclinations because they are non-orientable. This

[6] There may be other types of deformations which we choose to exclude due to energetic or other physical concerns. For instance, it might be convenient to consider deformations up to those which preserve the number of layers, which would prevent us from pushing the surfaces in the vertical direction.

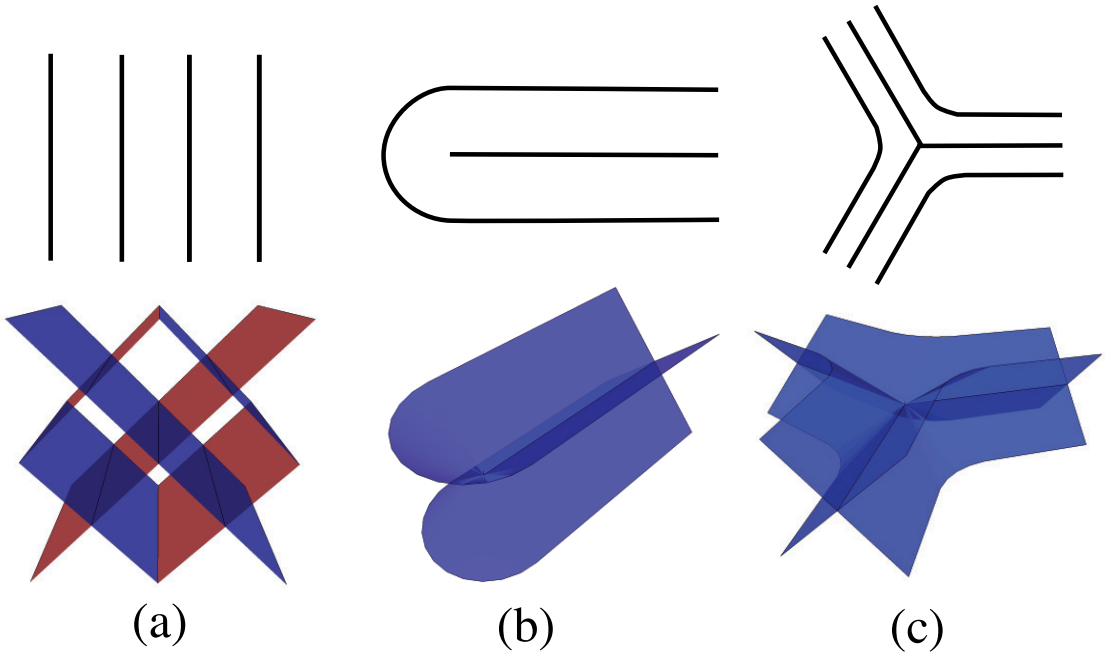

Figure 3.3: Examples of two-dimensional smectic configurations. The top row shows the layers derived from slicing the surface shown in the bottom row at integer values of the height, i.e. taking level sets. (a) ground state. Note the two sets of planes arising from the $\phi \to -\phi$ symmetry. (b) $+1/2$ index disclination. (c) $-1/2$ index disclination. These two unoriented singularities join the two sets of planes, so that one can no longer orient the layers as in Figure 3.1.

property arises because of their reflection symmetry $\phi \to -\phi$. Thus, in addition to the infinite set of planes normal to $(-\mathbf{k}, 1)$ in the line system, the smectic ground state also contains the infinite set of planes normal to $(\mathbf{k}, 1)$, as shown in Figure 3.3(a), since these generate the same set of unoriented layers. These two sets of planes intersect whenever ϕ is a half-integer multiple of a, which reflects the fixed points of the two symmetry operations $\phi \to \phi + a$ and $\phi \to -\phi$. Properly, for smectics ϕ is an element of the orbifold $S^1/\mathbb{Z}_2$, just as it was an element of S^1 for directed lines. At heights $ma/2$ then it is possible to cross continuously from one set of planes to the other, thereby changing the local orientation of the layers. Defects again connect the different planes together, although now this can be done in two different ways; either by connecting planes with the same orientation, as in the directed line system, or planes with the opposite orientation. The latter leads to a global non-orientability of the smectic and occurs when there are odd half-integer index disclinations. The two prototypical half-integer disclinations are depicted in Figure 3.3(b) $(+1/2)$ and Figure 3.3(c) $(-1/2)$. The $+1/2$ disclination consists of a pair of oppositely oriented planes terminated by a half-cone connecting them, while the $-1/2$ disclination is a three-way junction of pairs of oppositely oriented planes smoothly joined together. These examples provide a visual demonstration of the fact that odd half-integer index disclinations must have their singular points at $\phi = 0$ or $\phi = a/2$. Since these singular points terminate layers which connect the two sets of parallel planes, it follows that the layers must arise as projections from the fixed point values of ϕ – in other words, the presence of charge $1/2$ disclinations

forces the defect cores to sit at $\phi = na/2$, $n \in \mathbb{Z}$, or the heights of the level sets and halfway between them. We see that such disclinations can only occur at minima or maxima in the density of the smectic. No such restriction holds for the critical points with integer orientation degree, the consequence being that the saddle points in the directed smectic can lie at any phase value.

We may also choose to allow some slightly more singular events to occur, for instance the merging of defects or the climb of dislocations. In terms of the surfaces we can see that if two configurations differ in only a small patch whose boundary conditions agree, then they could be related by a local surgery event, where we take the patch in one surface and replace it with the patch from the other. These could be characterized by the bordism of configurations with defects (as defined in the introduction, augmented with the condition that now defects include not just discontinuities in ϕ but also $\nabla\phi$), which would also yield the extra information of how this process occurs in time.

Often we can determine whether such bordisms exist via the geometry of the height representation. For instance, consider the dislocation and the *pincement*. We are used to the idea that a disclination dipole creates a dislocation [Halperin and Nelson, 1978]. Indeed in Figure 3.4(a) we depict a $\pm 1/2$ disclination pair which form a charge $+1$ dislocation. However, consider the *pincement* shown in Figure 3.4(b). In this configuration the two singular points both lie at the *same* height and hence they can be cancelled. The smectic dislocation cannot be cancelled because

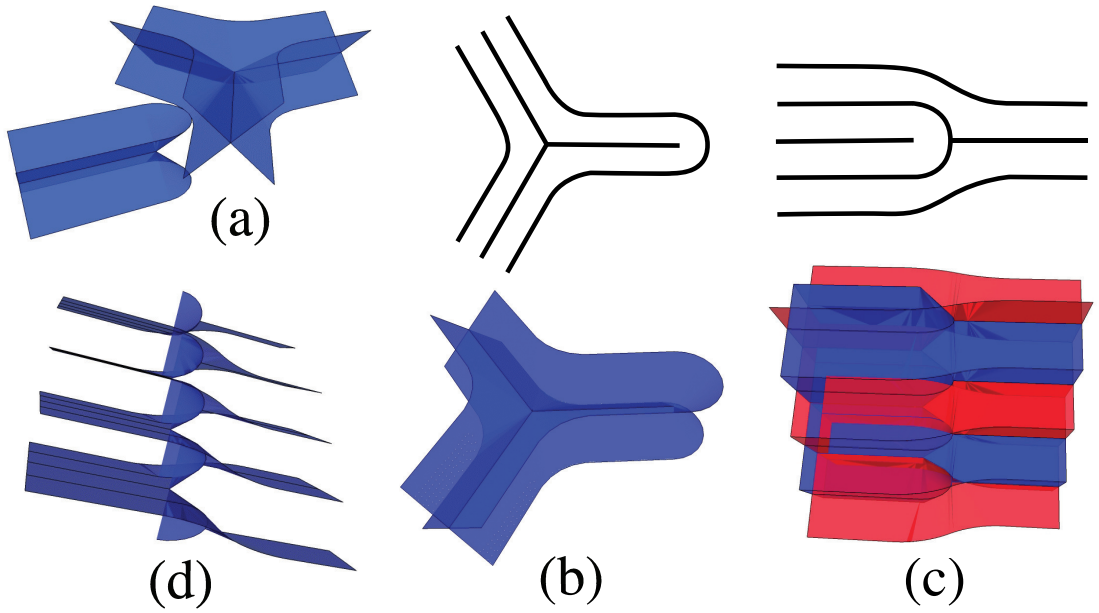

Figure 3.4: Disclination dipoles in smectics as examples of more complicated structures. (a) a $+1/2$ and $-1/2$ disclination pair forming a dislocation. For (b) and (c), the top row shows the layers derived from slicing the surface shown in the bottom row at integer values of the height, i.e. taking level sets. (b) pincement, formed from a disclination dipole where the singular points lie at the same height. (c) dislocation, also formed from a disclination dipole, but with the singular points at different heights. (d) a cutaway view of the helicoid sitting inside the dislocation.

the singular layers do not line up. Though this follows from the algebraic structure of paths on the Klein bottle, (*i.e.* $[S^{1/2}FS^{-1/2}]F^{-1} = S$, but $FF^{-1} = e$), the height construction provides a geometric way to see the difference between these two configurations. We are also able to construct a dislocation directly. Since a Burgers circuit around a dislocation changes ϕ by a multiple of a, it follows that the height function must be equivalent to a helicoid by a local surgery. As shown in Figures 3.4(c) and 3.4(d) the composite dislocation has the structure of two intertwined half-helicoids. Note that the charge of a dislocation depends on both the sign of the helicoid (left- or right-handed) and the tilt of the layers. A right-handed helicoid moved smoothly around a $+1/2$ disclination remains right-handed, but because the tilt of the layers has reversed the charge of the dislocation changes sign. This is the move that generates the ambiguity *modulo* 2 for the total dislocation charge in the presence of a $1/2$ index disclination [Kurik and Lavrentovich, 1988].

In order for dislocation/anti-dislocation pairs to form, a neck connecting adjacent surfaces must be formed. As long as this is smaller than the core size of the defects, it can be created without upsetting the overall topology. As the inchoate dislocation pair separates, these necks expand and, in a manner similar to continuous deformations of Riemann's minimal surface, break up into two oppositely handed helicoids [Colding and Minicozzi II, 2006] as depicted in Figure 3.1(c). Note that this type of process which necessarily includes local surgery for combining defects is implied in the theory of topological defects as well [Mermin, 1979]. In smectic systems, however, we must perform local surgery whenever we pull a defect through

a layer – this follows from the above result that the defect cores must remain at a constant height.

3.3 Jet bundles and contact structures

In this section, I will push a little further the idea of trying to start with a homotopy class on the torus or Klein bottle and get to a true 2D directed smectic or smectic defect behavior. First I will set up some formalism for keeping track of phase and gradient information simultaneously. Then I will show that the results of the homotopy theory of the naïve generalization are related to "formal solutions" to differential equations, i.e. solutions to the equations one gets by substituting formal variables for all derivatives in a differential equation. To get to homotopy theory of configurations, we will find that the constraint on paths

$$\frac{d\phi}{ds} = \nabla\phi \cdot \dot{\gamma} \tag{3.3.1}$$

forces us to look for formal solutions which respect a geometric object called a contact structure.

First we recall that in order to keep track of both translational and orientational order in a directed smectic system we had to consider not only ϕ but also $\nabla\phi$. We formalize this by introducing the space of 1-jets to ϕ. n-jets are simply a fancy term for the truncation of the Taylor series of a general function to nth order. We

can consider the space of all potential $1-$jets of a function at a point to be the Cartesian product of the space of possible values of the function with vector spaces for the possible gradients of each component of the function. For the 2D directed smectic and 2D smectic, the space of 1-jets is three dimensional with coordinates (ϕ, p_x, p_y), where p_x and p_y are potential values of $\partial_x\phi$ and $\partial_y\phi$.

Since $|\nabla\phi| = 0$ is a place where orientational order can no longer be defined, we should remove that line from this space. Then in the case of the directed smectic, we can find the torus that we generated in the naïve generalization by projecting curves in the 1-jet space onto the subset in this 1-jet space where $|\nabla\phi| = 1$.

Certainly every path in the configuration corresponds to some path in the 1-jet space. And we might hope that we could extend this one-way correspondence to homotopy classes; where perhaps not all homotopy classes of paths on the torus are realized by paths in the configuration. But none of this logic is reversible. In fact, if we keep only this information, we've already thrown away too much. Namely, we can no longer decide whether such curves are truly realizable in the sample, since we do not have enough information to check Eq. 3.1.1, which also includes $\dot{\gamma}$, the tangent of a curve in the sample.

Indeed, if we want to work with Eq. 3.1.1, we can't restrict ourselves to a single 1-jet space that we drag over the sample, but rather we really must keep a distinct copy over every point of the sample – we must consider a jet *bundle* over the sample space. The idea is somewhat like how one cannot naturally put tangent vectors

on different points of a curved surface in a single plane, but rather must consider different tangent planes at each point and then find ways to relate them afterwards. For the case of 2D directed smectic and smectic configurations, the jet bundles are 5 dimensional: two dimensions from the sample space, and three from the jet space. 2D directed smectic configurations $\phi(x, y)$ induce surfaces in this jet bundle, $(\phi(x, y), \partial_x\phi(x, y), \partial_y\phi(x, y))$. The winding of ϕ on a measuring loop on the surface gives a count of the dislocations inside the loop, and the winding of $\nabla\phi$ gives a count of the disclination charge inside. If orientational order and translational order were truly decoupled, arbitrary surfaces in this jet bundle would correspond to legitimate configurations, and we could thus construct e.g. disclinations of arbitrary positive charge. However, not every surface in the jet bundle arises from a configuration; consider for instance the plane $(\phi(x, y), p_x(x, y), p_y(x, y)) = (\phi_0, 1, 1)$. If $\phi(x, y)$ is constant, then p_x, p_y had better both vanish. Eq. 3.1.1 being true on any path is equivalent to the following differential form vanishing:

$$d\phi - p_x dx - p_y dy = 0. \tag{3.3.2}$$

I will explain now how the equation Eq. 3.3.2 places a geometric object on the jet bundle called a contact structure [Eliashberg and Mishachev, 2002], so that we can face more directly the obstruction to synthetically creating smectic configurations with arbitrary orientation fields and translation fields. I begin with a perverse way

of solving a differential equation. If we wanted to solve

$$0 = f\left(x, y, \frac{dy}{dx}\right), \tag{3.3.3}$$

we might first check that the equation

$$0 = f\left(x, y, p\right) \tag{3.3.4}$$

has solutions. Such a solution will be some implicit surface S in the 3-dimensional jet bundle with coordinates x, y, p. If this surface doesn't exist, then clearly the differential equation has no solutions. However, given this "formal solution", we still need to impose $p = dy/dx$ on it, which is implemented geometrically in the following way. The equation $p = dy/dx$, or equivalently $dy - pdx = 0$ is a relation between the components of a vector $a\mathbf{e}_x + b\mathbf{e}_y + c\mathbf{e}_p$ attached to a point (x, y, p). In particular, $b/a = p$. Geometrically, there is a two dimensional plane of vectors at each point in the jet bundle which can satisfy this equation, and these planes twist as p changes (as p increases, the slope dy/dx of the plane increases). Because of this twisting, not all of S can satisfy this condition, but one may be able to find curves on S which do. Such curves $(x, y(x), p(x))$ are solutions of the differential equation Eq. 3.3.3.

This odd way of solving a differential equation that we worked out above actually is what happens in the case of a 1D directed smectic, i.e. a phase function on the real line. We would simply replace the condition 3.3.3 by an Euler-Lagrange equation

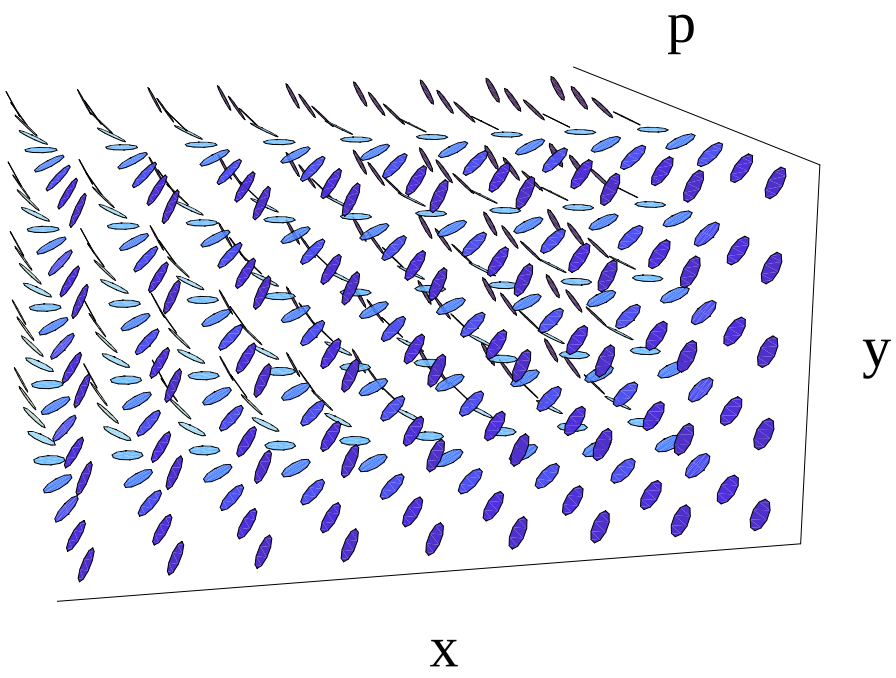

Figure 3.5: The contact structure on the jet space for an ordinary differential equation defined on the line. The contact planes twist along the p axis. In order for a formal solution to be a true solution, it must lie tangent to each plane.

for a suitable functional. Unfortunately, in this case where the dimensionality is low enough that we can actually draw pictures of the entire behavior of the configuration and its 1-jet, it hardly makes sense to talk about the orientation of a smectic in one dimension, and there are no interesting topological defects, either.

For the 2D directed smectic the story is higher dimensional but conceptually similar. The relation $d\phi - p_x dx - p_y dy = 0$ now gives us a 4-dimensional plane attached to every point in our 5-dimensional jet bundle. The 4-planes twist if either p_x or p_y change. The picture for an extension of a homotopy theory techniques to cover defects in smectics is clear though – one must consider homotopies which respect the contact structure. And because the contact structure is only defined in the full jet bundle, and not just the jet space alone, the allowed homotopies depend on the geometry of a path in the sample space.

This section has shown precisely what the naïve generalization of homotopy theory is missing. Having laid out the potential difficulties, I now list some reasons for hope. Despite seeming rather exotic, the study of curves tangent to a 3-dimensional contact structure has received a fair bit of attention in the low dimensional topology literature [Geiges, 2008]. There one of the goals is to understand the classification of Legendrian knots, or knots that lie tangent to a contact structure. It may be that methods there will be of use here.

3.4 Orbifolds

In light of the surface model, where defects were apparent as singularities in a 3-dimensional space (x, y, ϕ), it may seem perverse to have to consider the 5-dimensional space (x, y, ϕ, p_x, p_y) described in the previous section which arose from trying to repair naïve generalization ideas. In fact, those extra dimensions are only necessary if we inisit on trying to construct paths simultaneously in the translational order parameter and the orientational order parameter which are consistent with Eq. 3.3.2. We could alternatively just study the possible singularities of maps from the sample space to the phase space and simply let $\nabla\phi$ (and thus the orientational order) do what it will.

In section 3.2 it was noted that because of the reflection symmetry, the phase of the 2D smectic should be regarded as living in an *orbifold*, $S^1/\mathbb{Z}_2$. Orbifolds are spaces with singularities coming from points with "extra symmetries". In this section I will first discuss the geometry of crystallographic orbifolds and argue that they are the appropriate spaces for the phase fields of crystals. Next I will show how the singular points are well-adapted for disclinations in these defects. I will illustrate with examples from the 2D smectic and 2D square crystal.

Crystallographic orbifolds arise from tilings of Euclidean space (I will discuss here the line and the plane). Two simple examples are the tiling of the line by intervals and the tiling of the plane by parallelograms. In these two cases, the tiling

has a (discrete) symmetry group Γ which consists simply of translations – any point in a tile can be taken to an equivalent point in another tile by some sequence of translations. We can find a unit cell for the tiling by looking at the quotient space $\mathbb{R}^d/\Gamma$. Each geometrically distinct point in the tiling is parametrized by a point in this quotient space – and in these cases we get the circle and the torus. These spaces are both manifolds, meaning that every point in the space has a neighborhood which behaves like a piece of Euclidean space.

Now suppose that our tiling has symmetries. For the tiling of the line, suppose that the tiles have a reflection symmetry about their endpoints. This means that the symmetry group Γ now contains not only a translation, $T_a\phi = \phi + a$, but also a reflection $R\phi = -\phi$. The existence of one reflection implies the existence of reflections about all points $na/2$ as these can be written as the sequence $T_a R T_a^{-n}$. The unit cell which was an interval $[0, a]$ before now is $[0, a/2]$. Because of the reflection symmetries, if we were to stand in this unit cell and look around, it would be a bit like standing in a barber shop, with parallel mirrors on two walls. In particular, the points 0 and $a/2$ are now singular mirror points. This is the space we called $S^1/\mathbb{Z}_2$ earlier, as it is equivalent to a circle with points identified across an axis.

Let us now consider the case of a square tiling of the plane. I will now include a $\pi/2$ rotational symmetry about a corner of the pattern in the tiling group Γ. It can be checked algebraically this implies that Γ contains rotations of $\pi/2$ about

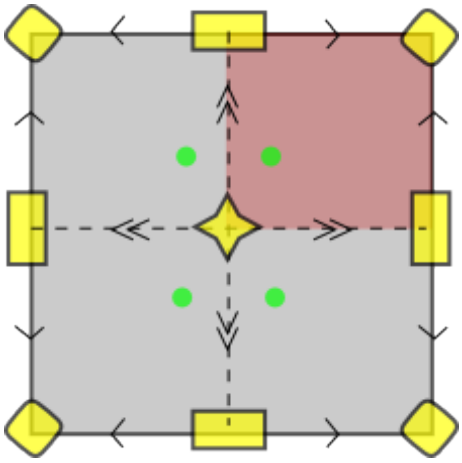

Figure 3.6: One square tile of a square lattice tiling with rotation by $\pi/2$ symmetry. The 4-pointed star is at the center of the tile, the diamond is at the corner, and the rectangle is at the midpoint of an edge. The green points are four points which are equivalent under a symmetry operation. A reduced unit cell is the upper right red square. If we identify the edges so that the arrows match up, we get the orbifold I call $X_{\square}$.

all corners and all centers of tiles, as well as rotations of π about the midpoints of edges. Geometrically, a unit cell of the tiling is now reduced to a square one-quarter the size of the tile (fig. 3.6). Consider a small neighborhood of the corner of the tile. Because of the four-fold rotational symmetry, there are four copies of points near the corner. After taking the quotient, we see that the corner is actually a cone point, with $\pi/2$ angle around it rather than 2π. There are a total of three singular points in the unit cell, the center of the tile and the corner become two cone points with an angle of $\pi/2$ and the midpoint of an edge of the tile is a cone point with an angle of π. This space is labelled $(2, 4, 4)$ after the orders of its cone points, I will call it $X_{\square}$.

Orbifolds are spaces that generalize manifolds. Points of orbifolds look like quotients of Euclidean space by a finite group of rotations or reflections. Above we saw

two types, mirror points in 1D and cone points in 2D. In two dimensions, mirror points can become mirror planes, and another type of singular point is possible where two mirror planes intersect, which are called corner reflectors. Some good references on orbifolds are Chapter 13 of Thurston [1980] and Chapter 13 of Ratcliffe [2006]. Johnson et al. [1996] emphasized the usefulness of orbifolds in crystallography, using them to draw pictures of space groups and interpret density functions, however did not discuss at all the implications for topological defects.

Order in crystalline systems is described by phase variables. For instance, for a 2D smectic we expand the density in Fourier components: $\rho(x, y) = \rho_0 + \rho_1 \cos \phi(x, y)$. Because cos is a periodic and even function, ϕ naturally lives on $S^1/\mathbb{Z}_2$. For a 2D square crystal, we might have $\rho(x, y) = \rho_0 + \rho_1(\cos(\phi_1(x, y)) \cos(\phi_2(x, y))$, where $\phi_1(x, y) = k_x x$ and $\phi_2(x, y) = k_y y$ in the ground state. The rotational symmetry that allow us to replace (ϕ_1, ϕ_2) with $(\phi_2, -\phi_1)$ means that (ϕ_1, ϕ_2) are coordinates on the space $X_\square$. (In fact, with this functional form for the density, the 2D square crystal has additionally some reflection symmetries, but we will ignore them here and below. A more appropriate form would place periodic functions with no reflection symmetry in place of each cos).

Orbifolds carry structure beyond the topology of their underlying spaces which keeps track of the tilings they arose from (or in general, covering spaces which respect the symmetries at the singular points). For instance, the underlying space of $S^1/\mathbb{Z}_2$ is simply an interval, which is contractible. The underlying space of $X_\square$

is a sphere. If the fundamental group of an orbifold were simply the fundamental group of the underlying spaces, this would tell us that neither of these systems could admit dislocations [7]. However, in both of the tilings modeled using these orbifolds it is possible to have dislocations and loops in samples with nonzero Burgers vector. Therefore we must consider loops which keep track of extra information. One way to understand this is to look at paths in the surface model in e.g. Fig. 3.3. The smooth curve on the surface $\phi(x, y)$ which projects to a loop in the xy plane surrounding a defect will in general not end at the original starting phase ϕ, but rather some value of ϕ related to it by a tiling group element (for smectics, some combination of reflections and translations). It turns out that this group element, the *holonomy*, is the same for any such "loop" on the surface in the same homotopy class [Ratcliffe, 2006]. Here the homotopy is such that we pin the starting and ending points so that they project to the same point in the sample. Furthermore if we compose paths, the holonomy of the paths is multiplied in order. This gives us a way of defining an orbifold fundamental group, and for crystallographic orbifolds, it's clear that this results in Γ.

Points in the sample mapped to cone points in the orbifold can have angles which are multiples of $\pi/2$ or π without introducing discontinuities. The order of the cone point is what determines the allowed amounts of excess or missing angle. We saw this already in the case of the 2D smectic, where $\pm 1/2$ disclinations had ϕ equal to half-integer multiples of a (Fig. 3.3). In the case of the 2D square crystal,

[7] I am using the homotopy theory of defects here for the dislocations, where it is completely valid.

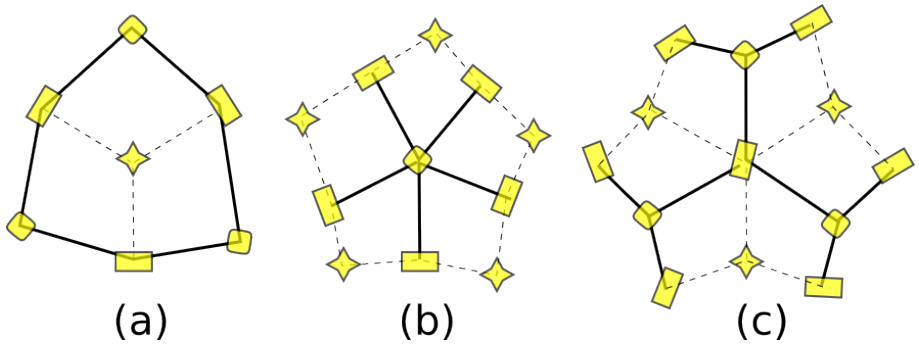

Figure 3.7: Disclinations in the square lattice can have their phase equal to any of the three singular points of $X_\square$. The notation is as in Fig. 3.6. (a) A disclination of "vertex" type where there is a vertex in the square tiling with coordination 3 rather than 4. (b) A disclination of "plaquette" type where there is a plaquette with 5 sides rather than 4. (c) A disclination of "edge" type where 3 tiles meet at the midpoint of an edge, instead of 2.

disclinations can be of three types, depending on the type of singular point they sit at: vertex type, plaquette type, and edge type. They are illustrated in Fig. 3.7.

Unfortunately I don't yet have a systematic way of understanding the possibilities for disclination defects in general examples yet. I will simply conclude this section by mentioning that just as we found the torus from the naïve generalization in the space of jets of S^1, the Klein bottle exists in the space of jets of $S^1/\mathbb{Z}_2$ as well (and in general crystalline systems, the space G/H from the naïve generalization can be found in the space of jets of whatever crystallographic orbifold is relevant to the ground state tiling). It's interesting at least how the singularities in the orbifold are resolved when looking at the space of jets. The space of jets of $S^1/\mathbb{Z}_2$ is a three-dimensional space, which we label with coordinates (ϕ, p_x, p_y) (Fig. 3.8). However, the ϕ axis does not trace out a circle, but an orbifold with fixed points at 0 and $a/2$. Therefore, we should look carefully at the planes $\phi = 0$ and $\phi = a/2$. In these planes, we identify $(p_x, p_y, 0)$ with $(-p_x, -p_y, 0)$ because when ϕ is identified

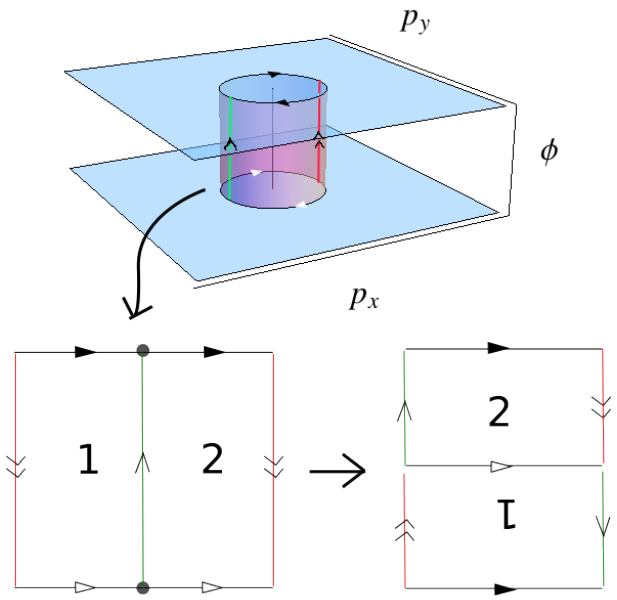

Figure 3.8: The top image shows the Klein bottle in the jet space of the 2D smectic as the cylinder $p_x^2 + p_y^2 = 1$. If we cut the cylinder along the red line and unroll it, we get the bottom left picture. Note that the top and bottom circles are drawn twice because of the reflection symmetry in the planes $\phi = 0, a/2$. We can then cut the left picture along the green line and reglue to get the picture on the right, which is the standard picture of the Klein bottle.

with $-\phi$ by a reflection, $\nabla\phi$ is identified to $-\nabla\phi$. Then a construction explained in Fig. 3.8 shows that the cylinder with $|\nabla\phi| = 1$ is a Klein bottle in this space.

3.5 Summary

We have outlined an approach to the study of topological defects in systems with broken translational invariance; topological equivalence requires more than just homotopic paths. One should consider homotopy classes of smooth(er) maps. Whereas the usual homotopy theory of defects would use continuous homotopy in the ϕ and θ components of the order parameter, we have argued that it is necessary to look

at homotopy of $\phi(\mathbf{x})$ and $\nabla\phi(\mathbf{x})$ together. Our method focuses on singularities and critical points in a phase field viewed as a height function over $\mathbb{R}^2$. Though the fundamental group of the ground state manifold can be constructed, it is known that when the loops involve both rotations and translations there are homotopy classes of loops implied that cannot be realized from configurations of the physical system. This arises from a mismatch of the dimensionality of the manifold of ground states with the number of Goldstone modes. To remedy this, we have constructed a local map from the configurations to the ground state manifold by employing Taylor series data at each point. We have shown that the homotopy theory of defects only works for singularities in ϕ (dislocations), and not consistently for singularities in $\nabla\phi$. Though the critical points in our theory behave somewhat like disclinations in nematics, they are not – as we demonstrated two +1 disclinations cannot be brought together.

Though we have focused here on two-dimensional smectics and directed lines, our approach easily generalizes to three-dimensional smectics which can be viewed as a height function over $\mathbb{R}^3$ into $S^1/\mathbb{Z}_2$. From this perspective the topological equivalence of edge and screw dislocations becomes particularly vivid; within the four-dimensional space spanned by (x, y, z, ϕ) the former are helicoids in x, y, ϕ for a fixed z, while the latter are helicoids in x, y, z at constant ϕ. Likewise, the theory of defects in solids can be formulated as maps from $\mathbb{R}^3$ to $T^3/\mathbb{X}$ where $\mathbb{X}$ is one of the 230 three-dimensional space groups. The dislocations will continue to correspond to cycles in the three components of the phase while the disclinations

will be correspond to the critical points of these maps.

What remains to be done is to systematize the body of knowledge regarding the topology defects in crystalline systems. In the case of directed lines, circle-valued maps of the sort we have described above are equivalent [Farber, 1995] to closed forms [Xing, 2009]. For unoriented lines, that line of formalism may best be extended by considering quadratic differentials instead [Strebel, 1984]. Combining these results with ours may lead to a way of extending our work to the topology of such patterns on surfaces of nontrivial topology (rather than just the plane). The layer normal of smectics on curved surfaces with planar topology can develop caustics [Santangelo et al., 2007]; extending our approach here to those systems is complicated by this additional holonomy and how it interacts with non-orientability near 1/2 disclinations. Thus the theory of defects for these systems should be given in the language of singularity theory [Golubitsky and Guillemin, 1973] and flavors of Morse theory [Milnor, 1964] which may combine those on circle-valued maps [Farber, 1995] and on singular spaces [Goresky and MacPherson, 1988]. While many of the mathematical concepts that are necessary may seem abstruse or abstract, this may be simply because they have been studied so far without the concrete motivation of understanding or imagining what happens to different types of defects in crystals or liquid crystals. Perhaps a materials perspective will also help to clarify the meaning of the mathematics, as well.

Chapter 4

Summary and Conclusion

In this work I have laid out the first steps and a few basic tools for the study of topological defects in liquid crystals beyond homotopy groups.

While the information from homotopy groups is helpful in many cases and certainly algebraically convenient, the layer of abstraction that one must undergo to convert from geometric to algebraic information can obscure how the interesting features in the particular sample are arranged. In chapter 2, I have applied the Pontryagin-Thom correspondence to give an alternate view of topology in nematic systems. The flavor of the constructions is such that instead of holding onto information at every point in a three-dimensional sample simultaneously, we can instead focus on some lower-dimensional sets and easily interpret how defects connect to one another. This representation of nematics exploits the fact that our visual systems

are well-adapted to handling two-dimensional surfaces in three dimensions. Beyond its intrinsic interest as a "calculational tool" that allows us to figure more directly what can happen to various complicated textures, one enticing possibility is the hope that one can now sculpt nematic configurations with interesting or useful features. Then boundary conditions on inclusions or interfaces that are consistent with the topology of a texture can be proposed directly and in a constructive fashion.

If the surfaces can be assigned an energy that is related to the elastic energy of the nematic (perhaps yielding an upper bound on the latter), then this strategy may even lead to new explicit families of ansatzes for nematic configurations given by specifying the behavior on surfaces. At the very least this would give new tools to the experimentalist or theorist attempting to estimate the energy cost of various regions in a given sample or simulation. The fact that the surfaces can be defined by looking at places where the director is perpendicular to some given orientation suggests that there may also be a relationship with the propagation of polarized light through the sample as well.

The work in Chapter 3 addressed long-standing misunderstandings and imprecisions in the literature on topological defects in smectics and crystalline systems. Although I have not yet reached a complete understanding of these defects (e.g. how to determine the result of merging arbitrarily knotted or linked disclinations and dislocations in a 3D crystal), I have identified some subtle features of the geometry which were not noticed or emphasized explicitly in the past. I showed that

the naïve generalization which relies on treating orientational and translational order independently can only be fixed if one considers the homotopy of such loops respecting a field of planes in the jet bundle of the sample. I also argued that the rotation and reflection symmetries in the point groups of crystalline systems naturally lead to singular spaces called orbifolds. Though crystals and smectics are typically drawn as configurations of lattices or layers in the sample, if one models them with continuous functions from the sample to phase variables which respect the symmetries of the system, one will find that the phases must have this orbifold structure. Furthermore, the discrete possibilities for the net change in orientation around a disclination in the sample correspond to the ways of packing neighborhoods of the singularities of the orbifolds around those points.

Let me end with some irresponsible speculation. One of the implicit messages of this work is that topological defects can combine in a multitude of ways (which I think of in terms of bordism operations) which cannot always be modeled with actions of homotopy groups. Is it possible to use topological defects in physical systems to change qualitatively the behavior of the material – are there exotic forms of strain hardening in general systems, for instance? In general what kind of information can be stored and manipulated with topological defects and how much of that can be programmed into elastic properties of the material? Another aspect of the theory of topological defects that I would like to understand better is how the defects change as the system passes through phase transitions and in particular whether the nature of the defects is important to the transition as in Kosterlitz and

Thouless [1973]; Halperin and Nelson [1978]; Lammert et al. [1993].

Bibliography

G. P. Alexander, B. G. Chen, E. A. Matsumoto, and R. D. Kamien. Disclination loops, hedgehogs, and all that in nematic liquid crystals. *Rev Mod Phys*, 84: 497–514, 2012.

M. V. Berry. Singularities in waves and rays. In R. Balian, M. Kléman, and J.-P. Poirier, editors, *Physics of Defects*, pages 453–549. North-Holland, Amsterdam, 1981.

S. Buoncristiano, C. P. Rourke, and B. J. Sanderson. *A geometric approach to homology theory*, volume 18 of *London Mathematical Society Lecture Note Series*. Cambridge University Press, Cambridge, 1976.

P. M. Chaikin and T. C. Lubensky. *Principles of Condensed Matter Physics*. Cambridge University Press, Cambridge, 1995.

B. G. Chen, G. P. Alexander, and R. D. Kamien. Symmetry breaking in smectics and surface models of their singularities. *Proc Natl Acad Sci*, 106:15577–15582, 2009.

T.H. Colding and W. P. Minicozzi II. Shapes of embedded minimal surfaces. *Proc Natl Acad Sci USA*, 88:11106–11111, 2006.

S. Copar and S. Zumer. Nematic braids: topological invariants and rewiring of disclinations. *Phys Rev Lett*, 106:177801, 2011.

P. G. de Gennes and J. Prost. *The physics of liquid crystals*, volume 83 of *International series of monographs on physics*. Second edition.

D. Deturck, H. Gluck, R. Komendarczyk, P. Melvin, C. Shonkwiler, and D. S. Vela-Vick. Pontryagin invariants and integral formulas for Milnor's triple linking number. *http://arxiv.org/abs/1101.3374*, 2011.

Y. Eliashberg and N. Mishachev. *Introduction to the h-principle*, volume 48 of *Graduate Studies in Mathematics*. American Mathematical Society, Providence, 2002.

V. Elser. A cubic Archimedean screw. *Phil Trans: Math, Phys, Eng Sci*, 354: 2071–2075, 1996.

M. Farber. *Topology of closed one-forms*. American Mathematical Society, Providence, 1995.

F.C. Frank. On the theory of liquid crystals. *Discuss Faraday Soc*, 25:11–28, 1958.

H. Geiges. *An introduction to contact topology*, volume 109 of *Cambridge Studies in Advanced Mathematics*. Cambridge University Press, Cambridge, 2008.

M. Golubitsky and V. Guillemin. *Stable Mappings and Their Singularities*. Springer-Verlag, New York, 1973.

M. Goresky and R. MacPherson. *Stratified Morse Theory*. Springer-Verlag, New York, 1988.

B. I. Halperin and D. R. Nelson. Theory of two-dimensional melting. *Phys Rev Lett*, 41:121–124, 1978.

A. Hatcher. *Algebraic Topology*. Cambridge University Press, Cambridge, 2002.

A. Henderson Squillacote. *The ParaView Guide: A Parallel visualization application*. Kitware, Inc., third edition, 2008. Software available at `http://paraview.org`.

D. A. Higgins and B. J. Luther. Watching molecules reorient in liquid crystal droplets with multiphoton-excited fluorescence microscopy. *J Chem Phys*, 119: 3935–3942, 2003.

K. Janich. Topological properties of ordinary nematics in 3-space. *Acta Appl Math*, 8:65–74, 1987.

C. K. Johnson, M. N. Burnett, and W. D. Dunbar. Crystallographic topology and its applications. *IUCr sponsored Macromolecular Crystallography Computing School*, `http://www.iucr.org/resources/commissions/crystallographic-computing/schools/school96/topology`, 1996.

M. Kléman and O. D. Lavrentovich. *Soft matter physics: an introduction*. Springer-Verlag, New York, 2003. pp. 447-452.

M. Kléman and L. Michel. Spontaneous breaking of euclidean invariance and classification of topologically stable defects and configurations of crystals and liquid crystals. *Phys Rev Lett*, 40:1387–1390, 1978.

J. M. Kosterlitz and D. J. Thouless. Ordering, metastability and phase transitions in two-dimensional systems. *J Phys C: Solid State Phys*, 6:1181–1203, 1973.

M. Kurik and O. D. Lavrentovich. Defects in liquid crystals: homotopy theory and experimental studies. *Sov Phys Usp*, 31:196–224, 1988.

P. E. Lammert, D. S. Rokhsar, and J. Toner. Topology and nematic ordering. *Phys Rev Lett*, 70:1650–1653, 1993.

T. Lee, R. P. Trivedi, and I. I. Smalyukh. Multimodal nonlinear optical polarizing microscopy of long-range molecular order in liquid crystals. *Opt Lett*, 35:3447–3449, 2010.

I. Low and A. V. Manohar. Spontaneously broken symmetries and Goldstone's theorem. *Phys Rev Lett*, 88:101602, 2002.

N. D. Mermin. The topological theory of defects in ordered media. *Rev Mod Phys*, 51:591–648, 1979.

L. Michel. Symmetry defects and broken symmetry. configurations hidden symmetry. *Rev Mod Phys*, 52:617–651, 1980.

J. Milnor. *Morse Theory*. Princeton University Press, Princeton, 1964.

J. Milnor. *Topology from the differentiable viewpoint*. Princeton University Press, Princeton, 1965.

J. F. Nye and M. V. Berry. Dislocations in waves. *Proc R Soc Lond A*, 336:165–190, 1974.

F. Obermeyer. Jenn3D: for visualizing Coxeter polytopes. *http://www.math.cmu.edu/~fho/jenn*, 2006.

V. Poénaru. Some aspects of the theory of defects of ordered media and gauge fields related to foliations. *Commun Math Phys*, 80:127–136, 1981.

V. Poénaru and G. Toulouse. The crossing of defects in ordered media and the topology of three-media. *J Physique*, 38:887–895, 1977.

H. Poincaré. *Papers on Topology: Analysis Situs and Its Five Suppplements*. American Mathematical Society, Providence, 2010. Translated by John Stillwell.

J. G. Ratcliffe. *Foundations of Hyperbolic Manifolds*, volume 149 of *Graduate Texts in Mathematics*. Springer-Verlag, New York, second edition, 2006.

D. Rogula. Large deformations of crystals, homotopy, and defects. In G. Fichera, editor, *Trends in Applications of Pure Mathematics to Mechanics*, pages 311–331. Pitman, London, 1976.

C. D. Santangelo, V. Vitelli, R. D. Kamien, and D. R. Nelson. Geometric theory of columnar phases on curved substrates. *Phys Rev Lett*, 99:017801, 2007.

J. P. Sethna and M. Huang. Meissner effects and constraints. In L. Nagel and D. Stein, editors, *1991 Lectures in Complex Systems*, pages 267–288. Addison-Wesley, 1992.

I. I. Smalyukh, Y. Lansac, N. A. Clark, and R. P. Trivedi. Three-dimensional structure and multistable optical switching of triple-twisted particle-like excitations in anisotropic fluids. *Nature Materials*, 9:139–145, 2009.

K. Strebel. *Quadratic differentials*. Springer-Verlag, New York, 1984.

J. C. Y. Teo and C. L. Kane. Majorana fermions and non-Abelian statistics in three dimensions. *Phys Rev Lett*, 104:046401, 2010.

W. P. Thurston. *The geometry and topology of three-manifolds*. unpublished Princeton notes, 1980. Available at `http://library.msri.org/books/gt3m/`.

U. Tkalec, M. Ravnik, S. Copar, S. Zumer, and I. Musevic. Reconfigurable knots and links in chiral nematic colloids. *Science*, 333:62–65, 2011.

T. tom Dieck. *Algebraic Topology*. European Mathematical Society, 2008.

J. T. Toner and D. R. Nelson. Bond-orientational order, dislocation loops and melting of solids and smectic-a liquid crystals. *Phys Rev B*, 24:363–387, 1981.

G. Toulouse and M. Kléman. Principles of a classification of defects in ordered media. *J Phys Lett*, 37:L149, 1976.

H.-R. Trebin. The topology of non-uniform media in condensed matter physics.. *Adv in Phys*, 31:195–254, 1982.

K. Volkert. Poincaré's cube manifolds. *Manifold Atlas*, 2011. Available at `http://www.map.him.uni-bonn.de/Poincar's_cube_manifolds`.

G. E. Volovik and V. P. Mineyev. Investigation of the singularities in superfluid ^{3}He in liquid crystals by the homotopic topology methods. *Zh. Eksp. Teor. Fiz. Pis'ma Red*, 24:605, 1976.

J. Wright and N. D. Mermin. Crystalline liquids: the blue phases. *Rev Mod Phys*, 61:385–432, 1989.

X. Xing. Topology and geometry of smectic order on compact curved substrates. *J Stat Phys*, 134:487–536, 2009.